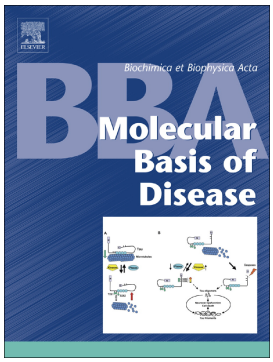

The MELAS mutation m.3243A>G promotes reactivation of fetal cardiac genes and an epithelial-mesenchymal transition-like program via dysregulation of miRNAs

Salvador Meseguer, Joaquin Panadero, Carmen Navarro-González, Magda Villarroya, Rachid Boutoual, Giacomo Pietro Comi, M.-Eugenia Armengod

PII: S0925-4439(18)30218-7
DOI: doi:10.1016/j.bbadis.2018.06.014
Reference: BBADIS 65161

To appear in: *BBA - Molecular Basis of Disease*

Received date: 21 February 2018
Revised date: 25 May 2018
Accepted date: 13 June 2018

Please cite this article as: Salvador Meseguer, Joaquin Panadero, Carmen Navarro-González, Magda Villarroya, Rachid Boutoual, Giacomo Pietro Comi, M.-Eugenia Armengod , The MELAS mutation m.3243A>G promotes reactivation of fetal cardiac genes and an epithelial-mesenchymal transition-like program via dysregulation of miRNAs. Bbadis (2018), doi:10.1016/j.bbadis.2018.06.014

The MELAS mutation m.3243A>G promotes reactivation of fetal cardiac genes and an epithelial-mesenchymal transition-like program via dysregulation of miRNAs

Salvador Meseguer[1*], Joaquin Panadero[2¶], Carmen Navarro-González[3¶], Magda Villarroya[4], Rachid Boutoual[5], Giacomo Pietro Comi[6], M.-Eugenia Armengod[7,8]

[1]RNA Modification and Mitochondrial Diseases Laboratory, Centro de Investigación Príncipe Felipe (CIPF), Carrer d'Eduardo Primo Yúfera 3, Valencia 46012, Spain. Electronic address: smeseguer@cipf.es.

[2]Unidad de Genómica, Instituto de Investigación Sanitaria La Fe, Avenida Fernando Abril Martorell, 106 Torre A 7ª planta, Valencia 46026, Spain. Electronic address: joaquin_panadero@iislafe.es.

[3]RNA Modification and Mitochondrial Diseases Laboratory, Centro de Investigación Príncipe Felipe (CIPF), Carrer d'Eduardo Primo Yúfera 3, Valencia 46012, Spain. Electronic address: cnavarrog@cipf.es.

[4]RNA Modification and Mitochondrial Diseases Laboratory, Centro de Investigación Príncipe Felipe (CIPF), Carrer d'Eduardo Primo Yúfera 3, Valencia 46012, Spain. Electronic address: mvillarroya@cipf.es.

[5]RNA Modification and Mitochondrial Diseases Laboratory, Centro de Investigación Príncipe Felipe (CIPF), Carrer d'Eduardo Primo Yúfera 3, Valencia 46012, Spain. Electronic address: rboutoual@cipf.es.

[6]Dino Ferrari Centre, Department of Pathophysiology and Transplantation (DEPT), University of Milan, I.R.C.C.S. Foundation Ca' Granda, Ospedale Maggiore Policlinico, via F. Sforza 35, 20122, Milan, Italy. Electronic address: giacomo.comi@unimi.it

[7]RNA Modification and Mitochondrial Diseases Laboratory, Centro de Investigación Príncipe Felipe (CIPF), Carrer d'Eduardo Primo Yúfera 3, Valencia 46012, Spain. Electronic address: marmengod@cipf.es.

[8]Centro de Investigación Biomédica en Red de Enfermedades Raras (CIBERER) node 721, Madrid 28029

***Corresponding author**

E-mail: smeseguer@cipf.es;

Phone: +34-963289680;

Fax: +34-963289701

¶These authors contributed equally to this work.

Abstract

The pathomechanisms underlying oxidative phosphorylation (OXPHOS) diseases are not well-understood, but they involve maladaptive changes in mitochondria-nucleus communication. Many studies on the mitochondria-nucleus cross-talk triggered by mitochondrial dysfunction have focused on the role played by regulatory proteins, while the participation of miRNAs remains poorly explored. MELAS (mitochondrial encephalomyopathy, lactic acidosis, and stroke-like episodes) is mostly caused by mutation m.3243A>G in mitochondrial $tRNA^{Leu(UUR)}$ gene. Adverse cardiac and neurological events are the commonest causes of early death in m.3243A>G patients. Notably, the incidence of major clinical features associated with this mutation has been correlated to the level of m.3243A>G mutant mitochondrial DNA (heteroplasmy) in skeletal muscle. In this work, we used a transmitochondrial cybrid model of MELAS (100% m.3243A>G mutant mitochondrial DNA) to investigate the participation of miRNAs in the mitochondria-nucleus cross-talk associated with OXPHOS dysfunction. High-throughput analysis of small-RNA-Seq data indicated that expression of 246 miRNAs was significantly altered in MELAS cybrids. Validation of selected miRNAs, including miR-4775 and miR-218-5p, in patient muscle samples revealed miRNAs whose expression declined with high levels of mutant heteroplasmy. We show that miR-218-5p and miR-4775 are direct regulators of fetal cardiac genes such as *NODAL*, *RHOA*, *ISL1* and *RXRB*, which are up-regulated in MELAS cybrids and in patient muscle samples with heteroplasmy above 60%. Our data clearly indicate that TGF-β superfamily signaling and an epithelial-mesenchymal transition-like program are activated in MELAS cybrids, and suggest that down-regulation of miRNAs regulating fetal cardiac genes is a risk marker of heart failure in patients with OXPHOS diseases.

Key Words: OXPHOS diseases; heteroplasmy; hypertrophic cardiomyopathy; miR-218-5p; miR-4775

1. Introduction

Mitochondria are pivotal organelles to eukaryotic cells. They play a crucial role in ATP production, via the oxidative phosphorylation (OXPHOS) system, and in several metabolic pathways, cell signaling and apoptosis [1-4].

Mitochondrial DNA (mtDNA) encodes 13 of the about 100 proteins that make up the OXPHOS system, and the 2 rRNAs and 22 tRNAs necessary for mitochondrial translation. The rest of the OXPHOS subunits and mitochondrial translation factors are encoded by the nucleus (nDNA). Therefore, defects in the OXPHOS system (OXPHOS diseases), which have extremely variable clinical manifestations, ranging from single-affected tissues to multisystemic syndromes, can be the result of both mtDNA and nDNA mutations [5-7]. The pathogenic mechanisms associated with OXPHOS dysfunction are not well-understood, but they likely involve retrograde signaling pathways, from mitochondria to nucleus, that are activated by changes in metabolite homeostasis, such as ROS, Ca^{2+}, ADP/ATP, and NAD/NADH, and impaired mitochondrial proteostasis [2, 8-11]. Retrograde signaling leads to adaptive/maladaptive changes in the expression of nuclear genes, which are modulated by cell-type and genetic and epigenetic factors.

Most studies on the pathomechanisms associated with OXPHOS dysfunction have focused on the role played by protein components, while the role of non-coding RNAs remains poorly explored [12-16]. MicroRNAs (miRNAs) are short, single-stranded, non-coding RNA molecules (19–23 nucleotides) that regulate gene expression through the binding within RNA-induced silencing complex (RISC) to their mRNA targets for degradation or repression of mRNA translation [17, 18]. They are implicated in a variety of physiological and pathological processes [19], and in the mitochondria-nucleus cross-talk [15]. In this respect, we have recently demonstrated, in cybrid models of different mtDNA diseases, that the expression of several nuclear-encoded mitochondrial proteins is modulated by miRNAs in response to changes in metabolite homeostasis, which apparently aggravates the cell phenotype [13, 14]. Therefore, it is reasonable to hypothesize that dysregulation of miRNA expression contributes to the clinical symptoms of OXPHOS diseases.

MELAS (mitochondrial encephalomyopathy, lactic acidosis, and stroke-like episodes) is a well-known example of mtDNA disease. Mostly caused by the m.3243A>G mutation in mitochondrial $tRNA^{Leu(UUR)}$ gene [20], it is a rare progressive multisystemic disorder (ORPHA:550; OMIM: 540000) with broad manifestations including encephalomyopathy, lactic acidemia, stroke-like episodes, dementia, epilepsy, recurrent headaches, hearing impairment, diabetes, heart disease, endocrinopathy, and short stature [20-23]. It was determined that the frequency of m.3243A>G in the general population is 0.14% [24], although the minimum point prevalence of clinically affected adults with this mutation is ~0.004% [25], as the phenotypic expression is ultimately dependent on the proportion of mutated mtDNA (heteroplasmy) within vulnerable tissues [11, 26]. The absolute amount of wild-type mtDNA, nDNA background, and epigenetic and external factors can also have an influence on phenotype [6, 27-31].

Cardiac and neurological diseases are the commonest causes of early death in MELAS patients carrying m.3243A>G [22]. In this respect, cohort studies using echocardiography have identified left ventricular hypertrophy (which still represents a major clinical predictor of heart failure and sudden cardiac death in humans [32]) in 34-56% patients [22, 33]. Notably, an electrocardiographic study revealed a correlation between skeletal muscle mutation load and indexed left ventricular mass [23], which suggests that patients with high levels of m.3243A>G mutation in skeletal muscle may be at increased risk of development of cardiomyopathy [22]. Moreover, a recent study carried out after two young, asymptomatic adults harbouring the m.3243A>G mutation died suddenly and unexpectedly revealed high levels of the mutation in both cardiac and skeletal muscle [26]. Thus, high mutation load in muscle may be a common feature between symptomatic and asymptomatic carriers, pending more detailed studies in the latter. The report by Ng and colleagues [26] suggested that sudden and unexpected death is not uncommon in young, asymptomatic adults carrying the m.3243A>G mutation, highlighting the need for cardiac surveillance and identification of new cardiac risk markers in the management of this genetic disease.

In the present study, we used 143B osteosarcoma cells harboring 100% m.3243A>G mutated mtDNA (MELAS transmitochondrial cybrids) to investigate

the participation of miRNAs in the mitochondria-nucleus cross-talk associated with mitochondrial dysfunction. Through miRNA sequencing and bioinformatics analysis, we found that expression of 246 miRNAs was significantly altered by the MELAS mutation (FDR $\leq$ 0.05), with 126 miRNAs being up-regulated and 120 down-regulated. Selected miRNAs were validated in muscle samples from MELAS patients, and the expression of a subset of down-regulated miRNAs was found to be inversely correlated with the heteroplasmy degree. We show that these miRNAs are regulators of genes involved in cardiac remodeling. This study identifies miR-4775 and -218-5p as biomarkers of cardiac remodeling, and likely of cardiovascular risk, in MELAS patients.

2. Materials and Methods

2.1 Materials

SB431542 was purchased from Sigma. Oligonucleotides (S1 Table) were also purchased from Sigma.

2.2 Cell culture

A transmitochondrial cytoplasmic hybrid (cybrid) line was previously generated [14] by polyethylene glycol-mediated fusion of platelets, derived from a patient carrying m.3243A>G mutation, with human osteosarcoma 143B cells lacking mtDNA (TK-) (ρ0 cells) as described [34]. Cybrid clones were obtained by culturing the fusion mixture in selective Dulbecco's modified Eagle's medium (DMEM) (Biological Industries, Kibbutz Beit Haemek, Israel) containing glucose (4.5 g/l), pyruvate (0.11 g/l), 10% dialyzed fetal bovine serum (FBS) (Invitrogen, Carlsbad, CA, USA) and 100 µg/ml BrdU (5-bromo-2-deoxyuridine; without uridine) to prevent growth of TK+ donor cells. DNA was extracted from selected clones and analyzed by polymerase chain reaction-restriction fragment length polymorphism (PCR-RFLP) to find cells containing 100% mutant mtDNA or the wild type counterpart (WT cybrids). The presence or absence of the mutation in the cells was periodically confirmed using a PCR-RFLP assay [35] and qPCR [36]. Cybrids and human HeLa cells were cultured in high glucose Dulbecco's modified Eagle medium (Gibco) containing 10% fetal bovine serum, 1 mM

sodium pyruvate, 100 U/ml penicillin, 100 µg/ml streptomycin, 2 mM glutamine and 1mM non-essential amino acids.

2.3 Small RNA library construction and Illumina sequencing

For RNA sequencing, we used wild type (3 independent samples) and MELAS (3 independent samples) cybrid cells (N = 6 in total). Total RNA was isolated using TRIzol Reagent (Life Technologies, Grand Island, NY, USA), and the quality of RNA was evaluated using the BioAnalyzer (Agilent, Santa Clara, CA, USA). RNA Integrity Number (RIN) ranged from 9.2 to 9.8. Small RNA libraries (small RNAs with 17–50 nucleotides) were constructed using the Solexa small RNA sample preparation protocol (Illumina, San Diego, CA, USA). Single-end 50nt bp read sequencing was performed using the Solexa HiSeq2000 platform (Illumina, San Diego, CA, USA) at Genomics unit of Centre for Genomic Regulation (Barcelona). We used 1 lane for the six samples. The raw sequencing data were deposited in NCBI's Gene Expression Omnibus (GEO) with the accession number GSE113300.

2.4 Program implementation

All sequencing software tools were run with the default or recommended settings under eight cores and 32GB of RAM computer. The operating system was Xubuntu 14.04.2 LTS (Long Time Support) using version of X_86 64 bits.

2.5 miRNA analysis

Reads quality and viability was checked using Fastqc software version 0.11.5, poor quality reads were trimmed and filtered out with cutadapt version 1.12. After trimming step, kept reads, were aligned against the Ensembl GRCh38 ncRNA database with Tophat2 version 2.1.1 (previously indexed with Bowtie2), classifying each, according the corresponding biotype (lincRNA, snRNA, snoRNA, miRNA, etc.). Reads aligned and classified as miRNAs, were kept and re-aligned against the hsa-hairpin.fasta file downloaded from miRBase database, for acute classification and expression level analysis. Expression level analysis was applied only on miRNAs (hairpins/mature) displaying a consistent number of sequences/reads (≥ 150) keeping only those showing a

False Discovery Rate (FDR) correction value lower than 0.05 after applying a Moderated t-statistics by LIMMA (Bioconductor). The raw data of miRNAs (hairpins/mature) (S4 and S5 Tables) and their expression level analysis (S7 and S8 Tables) were deposited in GEO (GSE113300). Hierarchical clustering was performed to visualize expression patterns of all differentially-expressed miRNAs. The normalized expression values were log2 transformed and unsupervised two-way hierarchical clustering was performed using Euclidean distance and weighted average linkage (WPGMA) to cluster miRNAs and samples.

For genomic localization, we downloaded miRNAs and chromosomal coordinates (chromosome, start, end, and strand) from Biomart available at Ensemble. miRNA cluster was defined as miRNA genes located within 10 Kb of distance on the same chromosome, the same criteria used by miRBase database.

Gene Set Enrichment Analysis (GSEA) was performed with potential target genes of those significant miRNAs according to TargetScan and following the procedure described in [37], obtaining the Biological Processes (BP), Molecular Functions (MF) and Cellular Components (CC) affected according the Gene Ontology Consortium (GO). mRNAs target for either up- or down-regulated miRNAs, and not for a mix of both types of miRNAs, were referenced as exclusive. By using GSE1462 (MELAS Muscle Tissue Biopsies) and GSE27545 (MELAS 143B osteosarcoma cybrids) datasets from database repository Gene Expression Omnibus (GEO), we identified among the exclusive targets, mRNAs whose expression change between WT and MELAS conditions.

2.6 Ethics statement

All muscle biopsies were provided by Telethon Network of Genetic Biobanks, which were collected from patients with MELAS disease and from healthy subjects. Written informed consent was obtained from the participants. All procedures were approved by the Ethics Committee of Milano Area 2, Fondazione IRCCS Ca' Granda Ospedale Maggiore Policlinico (Milan, Italy) and

performed in accordance with the guidelines set forth by the Declaration of Helsinki.

2.7 Heteroplasmy determination by qPCR

Detection and quantification of m.3243A>G mitochondrial point mutation in WT and MELAS cybrid cells, and muscle biopsies was performed as described [36]. Results are provided in S2 and S3 Tables.

2.8 Pre-miR transfection

Cybrid cells were seeded at 1,500,000 cells/100mm dish. After 24h, cells were transfected with one of Pre-miR miRNA Precursor Molecules (pre-miR-218-5p, pre-miR-4775 or Negative Control (NC)-pre-miR; Applied Biosystems) at the 50 nM final concentration, using Lipofectamine 2000 reagent (Invitrogen) and Opti-MEM medium according to the manufacturer's instructions. The medium was replaced by fresh growth medium after 6h of transfection and cells were collected after 48h of transfection.

2.9 Luciferase reporter assays

The 3′UTRs of *NODAL*, *RHOA*, *ISL1* and *RXRB* genes were amplified by PCR and cloned in sense (+) and antisense (-) downstream of the luciferase reporter gene into the XbaI site of the pGL3 Luciferase Reporter Vector (Promega). All Luciferase reporter plasmid constructs were verified by DNA sequencing. HeLa cells were seeded at 50,000 cells/well. After 24h, 500 ng of a Luciferase reporter plasmid and, as an internal control, 25 ng of Renilla Luciferase control vector (Promega) were co-transfected together with one of the RNA oligonucleotides at the 50 nM final concentration, using Lipofectamine 2000 reagent (Invitrogen) and Opti-MEM medium according to the manufacturer's instructions. After 48h, cells were lysed and Firely and Renilla luciferase activities from the cell extracts were measured with the Dual-luciferase Reporter Assay System (Promega) following the manufacturer's procedure.

2.10 RNA isolation and qRT-PCR

Total RNA from cybrid cells and muscle tissue samples was isolated using TRIzol reagent (Invitrogen). To quantify mRNA levels, one-step qRT-PCRs were performed in an Applied Biosystems Step-One Real-Time PCR System. 100 ng of total RNA were reverse-transcribed and amplified by qPCR in 12 µl of total volume reaction containing specific primers (Sigma) (S1 Table), Power SYBR Green PCR Master Mix, MultiScribe Reverse Transcriptase, and RNase Inhibitor (all from Applied Biosystems), according to the manufacturer's instructions. Amplification efficiency values were very near to 100%. Relative quantitation of mRNA levels was calculated using the comparative Ct method and ACTB gene as endogenous control. The absolute abundances of *NODAL*, *RHOA*, *ISL1* and *RXRB* mRNAs were estimated to be in a range of 2 to 775 copies/cell in 143B cybrid cells and of 1 to 4500 copies/cell in muscle samples by using equivalent calculations as described [14]. For miRNA quantification, 10 ng of total RNA were reverse-transcribed in 15 µl total reaction using the MultiScribe reverse transcriptase and specific stem-loop RT primers (Applied Biosystems). Then, 1.33 µL of cDNA was subjected to a TaqMan miRNA assay (Applied Biosystems), in a total reaction volume of 12 µL using specific primers and probes for the 20 selected human miRNAs and U6 snRNA, according to the manufacturer's protocol. Expression values were calculated using the comparative CT method and U6 snRNA as an endogenous control. We estimated the absolute abundances of miR-218-5p and miR-4775 to be at about 1500 and 160 copies/cell in 143B cybrid cells and muscle samples, respectively, following the formula described in [14]. The amounts of both miRNAs in the cell exceed the necessary threshold level of miRNA expression (100 copies /cell) proposed for significant target suppression [38].

2.11 Actin stress fiber staining

Actin cytoskeleton reorganization was assessed via filamentous actin (F-actin) staining using Rhodamine Phalloidin. The cells were fixed with 4% paraformaldehyde in PBS for 20 min at RT, washed with PBS, permeabilized with 0.3% Triton X-100 for 15 min at RT and washed again with PBS. Then cells were quenched in 100 mM NH4Cl, 150 mM glycine in PBS for 10 min and washed with PBS. Following blocking of nonspecific binding using 2% BSA,

0.05% Triton X-100 in PBS for 30 min at RT, the cells were stained with rhodamine-conjugated phalloidin (1:500 dilution in blocking solution, Sigma (P1951)) for 1h at 37ºC. Nuclei were counterstained with 0.1 µg/mL DAPI nuclear blue dye (Roche Diagnostics). Slides were mounted in FluorSave reagent (Calbiochem-Merck 4 Biosciences) and images were obtained using Leica DM6000 fluorescence microscope equipped with DM500 camera.

2.12 Western blot

Cell extracts were prepared in RIPA buffer (150 mM NaCl, 1% Nonidet P40, 0.5% sodium deoxycholate, 0.1% SDS and 50 mM Tris-HCl pH 8.0), containing 0.1 mM leupeptin and 1 mM phenylmethanesulphonyl fluoride. When phosphoproteins were to be analyzed, cell extracts were prepared in lysis buffer (10 mM NaCl, 1% Nonidet P40, 15% Glycerol, and 50 mM Tris-HCl pH 7.4), containing 1 mM phenylmethanesulphonyl fluoride, 0.1 mM leupeptin, 2 mM sodium orthovanadate, 100 mM sodium fluoride and 20 mM tetrasodium pyrophosphate. Proteins (150 µg) from the various lysates were separated by SDS/PAGE (10% acrylamide) and transferred to PVDF membranes (GE Healthcare, Amersham Biosciences). For immunodetection, we used commercial antibodies: mouse monoclonal anti-E-cadherin (sc-8426, Santa Cruz), anti-Vimentin (V6630, Sigma), rabbit polyclonal anti-Furin (sc-20801, Santa Cruz), mouse monoclonal anti-TGF-β3 (sc-166861, Santa Cruz), anti-Nodal (sc-373910, Santa Cruz), anti-TβR-II (sc-17799, Santa Cruz), anti-ActR-IIb (sc-390977, Santa Cruz), rabbit monoclonal anti-phospho-Smad2 (Ser465/467)/Smad3 (Ser423/425) antibody (8828S, Cell Signaling), mouse monoclonal anti-Smad2/3 (sc-133098, Santa Cruz), anti-SNAI1 (sc-271977, Santa Cruz), anti-pan Rac/Rac1 (sc-514583, Santa Cruz), anti-RhoA (sc-418, Santa Cruz), anti-ROCK1 (ab36746, Abcam), mouse monoclonal anti-RXRB (sc-742, Santa Cruz) anti-ISL1 (sc-390793, Santa Cruz) and anti-VDAC (sc-390996, Santa Cruz). The anti-rabbit (A6154) and anti-mouse (A4416) IgG-horseradish peroxidase-conjugated secondary antibodies were obtained from Sigma. Protein bands were quantified by densitometric analysis with an Image Quant ECL (GE Healthcare).

2.13 Statistical analysis

Statistical analysis was performed using Student's *t* test and was conducted using GraphPad Prism 7 (GraphPad Software, Inc, San Diego, CA). The statistically significant differences between the means were indicated by asterisks (*$p < 0.05$, **$p < 0.01$ or ***$p < 0.001$), and non-significant differences by n.s. The *t*-test was used because data followed a normal distribution (Shapiro-Wilk test, threshold 0.05).

3. Results

3.1 Small RNA landscape in MELAS and wild-type 143B cybrids

Small RNAs expressed in three biological replicates of MELAS and wild-type (WT) 143B cybrids were size selected (17-50 nt) from total RNA (S1 Fig). The small RNA libraries were constructed and sequenced by high-throughput sequencing (Illumina). The sequencing generated an average of 34,099,500 and 29,524,900 raw sequences for MELAS and WT samples respectively. After removal of adapters and low-quality reads, the analysis of small RNA libraries returned an average of 25,950,000 sequences for MELAS samples and 24,010,000 for wild-type samples. The size distribution of sequences in wild-type and MELAS libraries provided a significant higher number of 34- and 49-nt-long sequences in MELAS than WT libraries. Both series showed an average of length of 26 nt and a majority of sequences were comprised between 21 and 24 nt, being 22 nt the most frequent size (S2 Fig).

By indexing and mapping the small RNA sequences to the human reference non-coding RNA data set from Ensemble (GRCh.38.ncrna), we determined their origin and distribution in several classes of non-coding RNAs, including miRNAs. Only 46% and 60% of the, respectively, MELAS- and WT-derived sequences could be classified since not all the non-coding RNA classes are present in the GRCh.38.ncrna (e.g., cytosolic rRNAs and tRNAs are not included in this database). We observed that WT and MELAS samples were specially enriched in miRNA sequences (88.2-91.8%), followed by small nucleolar RNA (snoRNA) (3.5-4.8%) and long intergenic non-coding RNA

(lincRNA) sequences (1.8-2.8%) (Table 1). miRNAs were slightly but significantly less abundant in MELAS cybrids (88.2%) than in controls (91.8%). Sequences from mitochondrial transfer RNA (mt-tRNA) and ribosomal RNA (mt-rRNA) constituted 0.9-1.4 % and 0.8-1% of total sequences, respectively.

3.2 The MELAS mutation triggers an important and specific miRNA response in 143B cells

To identify known miRNAs present in the wild-type and MELAS libraries, the cleaned sequences were mapped to the sequence library of human precursor miRNAs (pre-miRNAs) and mature miRNAs (miRNAs) deposited in miRBase 20.0 (http://www.mirbase.org). A total of 963 different pre-miRNAs (S4 Table; GSE113300) and 905 different miRNAs (S5 Table; GSE113300) were identified in the six libraries.

First, we examined the 20 most abundant pre-miRNAs (S3A Fig) and miRNAs (S3B Fig) in WT and MELAS cybrids. We observed that 18 out of the 20 most abundant pre-miRNAs in the control cells (S3A Fig, left) were also among the 20 most abundant pre-miRNAs in the MELAS cybrids (S3A Fig, right). Likewise, 18 of the 20 most abundant miRNAs in WT cells (S3B Fig, left) were among the 20 most abundant miRNAs in MELAS cells (S3B Fig, right). The mismatched pre-miRNAs and miRNAs between WT and MELAS cells (black and red arrows in S3 Fig) showed expression changes that were statistically significant in all cases except for pre-miRNA-191 and miRNA-27a-3p (S6 Table). Notably, the differentially expressed miRNAs (miR-186-5p, miR-27b-3p, and miR-181b-5p) have been associated with epithelial to mesenchymal transition (EMT) processes [39-41] and myocardial responses [42, 43].

Second, we compared the expression of the overall pre-miRNA and miRNA species between MELAS and WT cells. 263 pre-miRNAs were significantly changed in MELAS cells (FDR $\leq$ 0.05), with 131 (49.8%) being up-regulated and 132 (50.2%) down-regulated (S7 Table; GSE113300), while 246 miRNAs were significantly altered (FDR $\leq$ 0.05), 126 (51.2 %) up-regulated and 120 (48.8%) down-regulated (S8 Table; GSE113300). Notably, 175 out of 246 miRNAs (71%) came from differentially-expressed pre-miRNAs (S9 Table),

suggesting that the remaining miRNAs represent species with a different generation-rate or stability than their precursors. Therefore, transcriptional and/or post-transcriptional regulatory mechanisms control the levels of specific miRNAs in response to the MELAS mutation. The genomic location of the transcriptionally-regulated miRNAs (S9 Table) indicated that they are homogeneously distributed among chromosomes (S4 Fig; S10 Table), and that about 20% are grouped in clusters (S5 Fig; S11 Table), which suggests that a portion of miRNAs are co-expressed.

Finally, the 246 differentially expressed miRNAs were submitted to unsupervised hierarchical clustering to construct a heat map based on log 2 gene expression fold-changes (MELAS vs WT) (Fig 1A). A positive log 2 value indicated up-regulation, and a negative log 2 value indicated down-regulation. The clustering clearly segregated the two groups of cells (Fig 1A, X-axis dendrogram) and visualized two main clusters corresponding to the up- and down-expressed miRNAs that were easily divisible into sub-clusters of potentially co-regulated miRNAs (Fig 1A, Y-axis dendrogram).

Briefly, our results showed an important dysregulation of miRNAs in MELAS cybrid cells that appears to be mediated by both transcriptional and post-transcriptional mechanisms.

3.3 RNAseq and RT-qPCR provide similar expression values for 20 selected miRNAs in MELAS cells

Expression of 20 differentially expressed miRNAs was verified by qRT-PCR. Ten up- and ten down-regulated miRNAs in MELAS cells were selected according to two independent criteria. On the one hand, we randomly selected 10 out of the 20 miRNAs with the highest fold changes and good abundance threshold (an average of at least 1000 reads in WT cells) (criterion 1, S12 Table). On the other hand, we selected 10 miRNAs with the highest numbers of predicted targets identified from a list of differentially expressed genes in MELAS cybrids and tissue samples, according to the database repository Gene Expression Omnibus (GEO). We only considered those cases where a gene appeared as a target for either up- or down-regulated miRNAs, and not for a mix of both types of miRNAs. These genes were referenced as “exclusive”

genes in our work (criterion 2, S13 Table). Unsupervised hierarchical clustering over the 20 selected miRNAs is shown in Fig 1B. The qRT-PCR results (Figs 1C and D) were consistent with those from the RNAseq analysis. This finding reinforced the reliability of the RNAseq data and, accordingly, the conclusion that miRNAs are deregulated as a consequence of the MELAS mutation.

3.4 Expression of certain miRNAs correlates with the heteroplasmy of the mutant mtDNA in muscle samples from patients

In order to evaluate whether the miRNA response in MELAS cybrids mirrored the miRNA response in patient's cells, we explored the expression of the 20 selected miRNAs (S14 Table) in muscle tissue samples from 5 MELAS patients (cohort 1) with heteroplasmy levels ranged between 53 and 76% (76, 75, 69, 61 and 53 %) (S2 Table). As shown in Figs 2A and B, 10 out of the 20 miRNAs (50%) followed in muscle samples a similar expression trend to that observed in MELAS cybrids, 7 being down-regulated (miR-598-3p, -218-5p, -4775, -1276, -340-5p, 27b-3p and -186-5p) and 3 up-regulated (miR-199a-3p, -181a-3p and -214-3p). We also noted that expression of a subset of the down-regulated miRNAs correlated with the heteroplasmy levels. In particular, we detected a statistically significant inverse correlation between the expression level of miR-598-3p, -218-5p, -4775, -27b-3p and -186-5p and the m.3243A>G mutation load in muscle (Figs 2C and D; S15 Table); i.e., the higher level of mutation load, the lower expression of the miRNAs. No significant correlation was observed for the up-regulated miRNAs (Fig 2E; S16 Table).

To confirm the inverse correspondence of the miR-598-3p, -218-5p, -4775, -27b-3p and -186-5p expression levels with the m.3243A>G mutation load, we introduced in our analysis a new cohort of 9 MELAS muscle samples (cohort 2) with heteroplasmy levels ranged between 49 and 72% (S3 Table) and 3 controls. We found that in the total sample pool (cohort 1 plus cohort 2) the 5 miRNAs kept a low expression level (Fig 2F), and 3 of them (miR-598-3p, -4775 and -218-5p) still showed a significant inversed correlation with m.3243A>G mutation load (Fig 2G; S17 Table).

Altogether our data suggest that MELAS cybrid cells and muscle tissue from MELAS patients share a set of dysregulated miRNAs, and specifically

point to down-regulation of miR-598-3p, -218-5p, -4775, -27b-3p and -186-5p as a hallmark of MELAS. Notably, a recent report identified miRNA-27b-3p as a putative biomarker for MELAS diagnosis [16]. In that report, a significant inverse correlation was found between serum miR-27b-3p and lactate, the Newcastle Mitochondrial Disease Scale for Adults (NMDAS), and m.3243A>G mutation load in muscle. Therefore, miR-27b-3p appeared to decrease with the clinical severity of MELAS patients. In our study of muscle samples, we found a significant inverse correlation between the expression of miR-598-3p, -218-5p and -4775 and the m.3243A>G load, whereas inverse correlation was of borderline statistical significance (p=0.067) in the case of miR-27b-3p. miR-218-5p and miR-4775 were chosen for further studies as their inverse correlation with m.3243A>G load provided the lower p values.

3.5 The MELAS mutation increases the expression of *NODAL*, *RHOA*, *ISL1* and *RXRB* via down-regulation of miR-218-5p and miR-4775

To explore the biological significance of miR-4775 and -218-5p down-regulation in MELAS cells, we first performed a functional analysis of the 246 differentially-expressed miRNAs in MELAS cybrids and then we looked at which functional packages the two selected miRNAs were related to. We used TargetScan for predicting target genes of the 246 differentially expressed miRNAs (S18 Table), and Gene ontology [GO] for their functional annotation (S19 Table). Enrichment analysis of GO terms showed 147 enrichment items of biological process (S19A Table), including several packages related to muscle and nervous system development, 32 of molecular function (S19B Table) and 22 of cellular components (S19C Table).

Particularly interesting was the association with functional packages related to heart and signaling pathways controlling cardiac events (some examples for the three GO subcategories (biological process, molecular function and cellular component) are highlighted in black bold in S19A, S19B and S19C Tables, respectively). Structural and functional abnormalities of the heart are common in MELAS patients with the m.3243A>G mutation [22, 23, 33, 44, 45], and the presence of cardiomyopathy worsens the prognosis of these patients because it is associated with increased mortality [46, 47]. Moreover, in

MELAS patients with left ventricular hypertrophy, a significant correlation was observed between the ratio of left ventricular mass to body surface area and the degree of the mutation heteroplasmy [23]. Although the mechanisms of left ventricular hypertrophy in MELAS remain unclear [44], reactivation of fetal genes driven by miRNAs has been involved in pathological cardiac remodeling [32, 43]. Notably, our analysis provided multiple target predictions for miR-4775 and -218-5p within functional packages related to heart and signaling pathways controlling cardiac events, including cardiac development (S20 Table). This finding suggests that both miRNAs could be involved in cardiac events associated with MELAS.

To explore the role of miR-4775 and -218-5p in the reactivation of genes involved in cardiac remodeling and development, we selected four “exclusive” target genes from GO items related to these processes: *NODAL*, *RHOA*, *ISL1*, and *RXRB* (S21 and S22 Tables). NODAL and RHOA are associated with the TGF-β signaling pathway (Fig 3), which is involved in epithelial-mesenchymal transitions (EMTs) operating in heart development and disease [48-59]. NODAL is a member of the TGFβ superfamily and, therefore, acts as activator of the pathway, whereas RHOA is a downstream effector that induces the formation of actin stress fibers during TGF-β-induced EMT. ISL1 and RXRB are key transcriptional regulators of the cardiac progenitor cell lineage [60-64]. Interestingly, we found that the mRNA and protein levels of the four selected genes were increased in MELAS cybrids, showing therefore an opposite expression pattern to their putative regulatory miRNAs, miR-218-5p and miR-4775 (Figs 4A and B, Figs 5A and B, and Fig 1C).

Anti-correlated expression of miR-218-5p and miR-4775 respect to their putative target genes was confirmed by transfecting WT cells with appropriate pre-miR mimics. Transfection with pre-miR-218-5p reduced the expression of *NODAL* and *RHOA* respect to the control at both mRNA and protein levels (Figs 4C and D), whereas transfection with pre-miR-4775 reduced the expression of *ISL1* and *RXRB* at mRNA and protein levels in relation to the control (Figs 5C and D). Moreover, a decrease in the expression of the target genes was observed after transfection of MELAS cybrids with the pre-miR mimics (Figs 4E, 4F, 5E and 5F).

Furthermore, we explored the capability of miR-218-5p and miR-4775 to bind to the 3'UTR of their predicted mRNA targets by means of a luciferase reporter assay [65]. To this end, we cloned the 3'UTR of each mRNA in direct (+) or reverse (-) direction downstream of the luciferase reporter gene. Then, we co-transfected each recombinant plasmid into HeLa cells together with the respective pre-miR or its negative control (NC-Pre-miR) and determined the luciferase activity. As shown in Fig 4G and 5G, the cotransfection of each reporter (+) with the corresponding pre-miR significantly reduced the luciferase activity when compared with the NC-pre-miR-transfected cells, whereas no effect was observed when the reporters carried the 3'UTR cloned in the reverse direction (-). Altogether these data indicate that miR-218-5p directly targets *NODAL* and *RHOA* (Fig 4G) and that miR-4775 directly targets *ISL1* and *RXRB* (Fig 5G).

3.6 The MELAS mutation triggers a miRNA-mediated cardiac remodeling program via TFG-β superfamily signaling and reactivation of fetal cardiac genes

In MELAS cybrids, we also observed an increased expression of other members of the TGF-β superfamily, such as TGF-β3 and BMP4 (Fig. 6A and B), which are putative targets of different down-regulated miRNAs (S20 Table, highlighted in red bold). In contrast, no changes were detected in the mRNA expression of Lefty1 and Lefty2 (Fig 6A), which act as extracellular antagonists of NODAL signaling [66], and myostatin (MSTN), a member of the TGF-β superfamily that acts as a negative regulator of muscle growth [67]. The increased expression of NODAL, TGF-β3 and BMP4 is likely responsible for the activation of TGF-β superfamily signaling (as revealed by the up-regulation of the TGF-β convertase Furin, which is transactivated by TGF-β signaling through the p42/p44 MAPK pathway [68], and the TGF-β type II receptors TβR-II and ActR-IIb, the phosphorylation and activation of Smad2/3, and the up-regulation of SNAI1, ROCK1 and Rac1; see Figs 6B and C) and of an EMT-like program [51, 56, 69] (as indicated by the up-regulation of the mesenchymal markers vimentin and N-cadherin, and down-regulation of the epithelial marker E-cadherin; see Figs 6D and E). That TGF-β superfamily signaling is activated in

MELAS cybrids was further supported by the findings that treatment of these cells with the TGF-β inhibitor SB431542 (which is an inhibitor of TGF-β type I receptors; [70]) or transfection of MELAS cells with pre-miR-218-5p (which negatively regulates the *NODAL* expression; see Fig 3) led to a decrease in phosphorylation of SMAD2/3 and/or the SNAI1 levels (Figs 7A and B).

TGF-β signaling induces mobilization of actin cytoskeleton via small GTPases such as RHOA and RAC1 (Fig 3), a process that has been associated with ventricular myocyte hypertrophy and, consequently, with pathogenic cardiac remodeling [48, 49, 57, 71]. Interestingly, we observed that the MELAS cybrids contain many filamentous bundles organized as stress fibers, as recently described [72], and that treatment with the TGF-β inhibitor SB431542 abrogated this organization of the actin filament system (Fig 6F and G). Similarly, the transfection with pre-miR-218-5p, but not with pre-miR-4775, greatly reduced the stress fiber formation (S6 Fig). These data indicate that induction of TGF-β signaling promotes reorganization of the actin cytoskeleton in MELAS cybrids, which could occur via the RHOA/ROCK1 pathway, and that miR-218-5p plays an important role in this process (see Fig 3).

On the other hand, transfection of MELAS cybrids with pre-miR-4775 led to a decrease in the expression of the fetal cardiac genes *MEF2C* and *TNNT2* (Fig 7C), which are targets of ISL1 [73, 74].

Altogether these results indicate that, in cybrid cells, the MELAS mutation promotes expression of genes involved in cardiac remodeling through a miRNA-mediated activation of both TGF-β superfamily signaling and genes involved in cardiac development. Notably, in patient muscle samples, we observed an increase in the NODAL, RHOA, ISL1, MEF2c, and RXRB mRNA levels when the mutation load was higher than 60% (Fig 8), which is a reminiscent trait of that exhibited by MELAS cybrids (100% heteroplasmy). These data suggest that down-regulation of miR-218-5p and miR-4775 in muscle samples associated with a mutation load higher than 60% may be a risk marker for heart failure in MELAS patients.

4. Discussion

In this work, we demonstrated that the MELAS mutation m.3243A>G triggers an important and specific miRNA response in 143B cells, which highlights the role of miRNAs in the cell response to mitochondrial dysfunction and, therefore, in the mitochondria-nucleus cross-talk. Using small RNAseq analysis, we identified 246 dysregulated miRNAs (FDR $\leq$ 0.05), with 126 (51.2 %) being up-regulated and 120 (48.8%) down-regulated. Reliability of the RNAseq data was confirmed by qRT-PCR analysis of 20 miRNAs. We used TargetScan for predicting target genes of the 246 differentially expressed miRNAs, and Gene ontology [GO] for their functional annotation. The enrichment analysis revealed that target genes for dysregulated miRNAs were associated with GO items related to muscle and nervous system development, heart, and signaling pathways controlling cardiac events. This finding suggests that the miRNA program triggered by the MELAS mutation could explain for some of the clinical manifestations of the MELAS syndrome.

We observed that 5 out of 10 selected, down-regulated miRNAs (miR-598-3p, -218-5p, -4775, -27b-3p and -186-5p) in MELAS cybrids also exhibited a significant lower expression in muscle samples from 14 MELAS patients relative to 6 controls, and that 3 of them (miR-598-3p, -4775 and -218-5p) showed a significant inversed correlation with the m.3243A>G mutation load; i.e., the higher mutation load, the lower expression of the miRNAs. Given that the incidence of major clinical features associated with the m.3243A>G mutation, including left ventricular abnormalities, has been correlated to the level of mutant mtDNA in skeletal muscle [23, 75], our data suggest that the low expression of miR-598-3p, -4775 and -218-5p in muscle may be a risk factor for severe symptoms of MELAS disease.

We demonstrate that miR-218-5p directly targets *NODAL* and *RHOA*, while miR-4775 directly targets *ISL1* and *RXRB*. Therefore, down-regulation of both miRNAs in MELAS cybrids is likely a major cause of the increased expression of NODAL, RHOA, ISL1 and RXRB in these cells. NODAL signaling is essential for the induction and pattering of mesoderm and endoderm during embryogenesis, and thus it is important to promote cardiogenic differentiation [66, 76-79]. RHOA has been shown to be essential in mammalian cardiac development [80, 81]. ISL1 has a hierarchical role in cardiac progenitor cells, regulating downstream genes by an epigenetic mechanism [64]. Finally, many

studies have demonstrated that the formation of the heart depends on retinoic acid signaling, which controls the activity of retinoic acid receptors, including RXRB [63]. Therefore, we conclude that by lowering the expression of miR-218-5p and miR-4775, the MELAS mutation promotes the reactivation of a fetal cardiac gene program including *NODAL*, *RHOA*, *ISL1* and *RXRB* (Fig 3).

In MELAS cybrids, we also observed induction of other recognized fetal cardiac genes, such as *BMP4* and *TGFB3* [32, 82], which are putative targets of down-regulated miRNAs identified in this study. Previous reports have established essential roles for miRNAs in cardiac hypertrophic and heart failure, although limited information is available about specific miRNAs that are involved in regulation of cardiac genes during both embryonic development and heart failure [32, 43]. Our work reveals new miRNAs involved in reactivation of fetal cardiac genes. In this case, unlike other studies, the primary cause of the reactivation is a mtDNA mutation and its associated mitochondrial dysfunction. It is possible that different causes leading to heart failure do it by reactivating different miRNA-driven programs of fetal cardiac genes. Mitochondrial cardiomyopathy has been described as a myocardial condition characterized by abnormal heart-muscle structure, function, or both, secondary to genetic defects involving the mitochondrial respiratory chain, in the absence of concomitant coronary artery disease, hypertension, valvular disease, or congenital heart disease [83]. Therefore, it seems reasonable to think that although sharing miRNAs with other causes of cardiomyopathy, mitochondrial cardiomyopathy has specific miRNA program(s).

As aforementioned, reactivation of fetal genes is thought to play a causative role in pathological cardiac remodeling and adult heart failure [32, 43, 84]. Specifically, cardiac hypertrophy has been associated with the reactivation of a fetal gene program including cardiac transcription factors, such as SMAD and MEF2 factors, and requiring the participation of small GTPases like RHOA [84, 85]. Notably, we found an increased expression of pSMAD2/3, MEF2C and RHOA in MELAS cybrids. Thus, it is reasonable to suspect that the reactivation of fetal cardiac genes in MELAS cybrids is related to an adverse cell response to mitochondrial dysfunction. Interestingly, we also observed increased mRNA levels of NODAL, RHOA, ISL1, MEF2C and RXRB in muscle samples from MELAS patients when the mutation load was higher than 60%, which was

commonly associated with low expression levels of miR-218-5p and miR-4775. Therefore, down-regulation in muscle of miRNAs controlling the expression of fetal cardiac genes, such as miR-218-5p and miR-4775, appears to be a risk marker for heart failure.

Our data clearly indicate that TGF-β superfamily signaling is activated in MELAS cybrids. TGF-β is a potent inducer of EMT, a complex process that allows a polarized epithelial cell to acquire a variety of mesenchymal phenotypic traits [86-88]. While being a fundamental process during development, EMT is recalled under pathological conditions, including heart disease [52, 53, 89]. SNAI1 is considered a key organizer of EMT, as it is involved in down-regulation of an important caretaker of the epithelial phenotype, *E-cadherin*, and in the activation of genes that contribute to the mesenchymal phenotype such as *N-cadherin* and *vimentin* [51, 56]. Complementing its signaling through SMADS (Fig 3), TGF-β also induces signaling through RHO-like GTPases, which regulate actin dynamics and control actin rearrangement during EMT [51]. Specifically, RHOA promotes formation of actin stress fibers, which are thought to increase cell contractility. Our data indicate that activation of TGF-β superfamily signaling in MELAS cybrids leads to a reorganization of the actin cytoskeleton, induction of SNAI1, down-regulation of E-cadherin, and increased expression of mesenchymal markers like vimentin and N-cadherin. Therefore, the MELAS mutation triggers an EMT-like process in 143B cells through activation of TGF-β superfamily signaling, which is mediated by down-regulation of miR-218-5p and miR-4775 (Fig 3).

Owing to critical dependence of the heart on oxidative metabolism, cardiac involvement in OXPHOS diseases is common and an important predictor of morbidity and early mortality [22, 46, 90]. Further studies in larger prospective cohorts are needed to clarify the role of miRNAs in the clinical features of cardiac involvement in MELAS and other OXPHOS diseases.

In brief, our data provide the first evidence of a miRNA program that promotes reactivation of fetal cardiac genes and an EMT-like process in response to a pathological mtDNA mutation.

5. Conclusions

Our study provides cutting-edge information on the involvement of microRNAs (miRNAs) in the cell response to the mitochondrial dysfunction associated with mutation m.3243A>G. Enrichment analysis revealed that target genes of dysregulated miRNAs were associated with GO items for muscle and nervous system development, heart, and signaling pathways controlling cardiac events. These findings point to a key role of miRNAs in mediating some of the clinical manifestations of MELAS. Validation of selected miRNAs in patient muscle samples allowed us to identify miRNAs, including miR-4775 and -218-5p, whose expression declines with increasing levels of the mutant mtDNA in skeletal muscle. We demonstrate that down-regulation of these miRNAs leads to reactivation of fetal cardiac genes and an epithelial-mesenchymal transition-like process, which are considered hallmarks of pathological cardiac remodeling. Since cardiac disease is one of the commonest causes of early death in m.3243A>G patients, low levels of certain miRNAs identified in this work may be a risk signature of heart failure in MELAS patients.

Competing interests

The authors declare that they have no competing interests.

Author contribution

S.M. and M.-E.A. and designed the study. S.M., C.N.-G., M.V. and R.B. performed the experiments. J.P. performed the bioinformatic analysis. G.P.C. provided the muscle samples and contributed to the analysis and interpretation of data. S.M. and M.-E.A wrote the paper. All authors reviewed the manuscript.

Funding

This work has been supported by grant BFU2014-58673-P from the Spanish Ministry of Economy and Competitiveness to M.-E.A.

Acknowledgements

The authors thank Dr. E. Knecht, Dr. C. Aguado, Dr. M.P. Rubio, Dr. A. Fathinajafabadi and Dr. R. Farràs (CIPF, Valencia, Spain) for their valuable advice and for providing facilities in our research work.

References

1. Nunnari J, Suomalainen A. Mitochondria: in sickness and in health. Cell. 2012;148(6):1145-1159. doi: 10.1016/j.cell.2012.02.035.
2. Reinecke F, Smeitink JA, van der Westhuizen FH. OXPHOS gene expression and control in mitochondrial disorders. Biochim Biophys Acta. 2009;1792(12):1113-1121. doi: 10.1016/j.bbadis.2009.04.003.
3. Chandel NS. Mitochondria as signaling organelles. BMC Biol. 2014;12:34. doi: 10.1186/1741-7007-12-34.
4. Tait SW, Green DR. Mitochondria and cell signalling. J Cell Sci. 2012;125(Pt 4):807-815. doi: 10.1242/jcs.099234.
5. Boczonadi V, Horvath R. Mitochondria: impaired mitochondrial translation in human disease. Int J Biochem Cell Biol. 2014;48:77-84. doi: 10.1016/j.biocel.2013.12.011.
6. DiMauro S, Schon EA, Carelli V, Hirano M. The clinical maze of mitochondrial neurology. Nat Rev Neurol. 2013;9(8):429-444. doi: 10.1038/nrneurol.2013.126.
7. Rotig A. Human diseases with impaired mitochondrial protein synthesis. Biochim Biophys Acta. 2011;1807(9):1198-1205. doi: 10.1016/j.bbabio.2011.06.010.
8. Cagin U, Enriquez JA. The complex crosstalk between mitochondria and the nucleus: What goes in between? Int J Biochem Cell Biol. 2015;63:10-15. doi: 10.1016/j.biocel.2015.01.026.
9. Chen C, Chen Y, Guan MX. A peep into mitochondrial disorder: multifaceted from mitochondrial DNA mutations to nuclear gene modulation. Protein Cell. 2015;6(12):862-870. doi: 10.1007/s13238-015-0175-z.
10. Dogan SA, Pujol C, Maiti P, Kukat A, Wang S, Hermans S, et al. Tissue-specific loss of DARS2 activates stress responses independently of respiratory chain deficiency in the heart. Cell Metab. 2014;19(3):458-469. doi: 10.1016/j.cmet.2014.02.004.
11. Picard M, Zhang J, Hancock S, Derbeneva O, Golhar R, Golik P, et al. Progressive increase in mtDNA 3243A>G heteroplasmy causes abrupt transcriptional reprogramming. Proc Natl Acad Sci U S A. 2014;111(38):E4033-4042. doi: 10.1073/pnas.1414028111.
12. Chinnery PF, Elliott HR, Hudson G, Samuels DC, Relton CL. Epigenetics, epidemiology and mitochondrial DNA diseases. Int J Epidemiol. 2012;41(1):177-187. doi: 10.1093/ije/dyr232.
13. Meseguer S, Boix O, Navarro-Gonzalez C, Villarroya M, Boutoual R, Emperador S, et al. microRNA-mediated differential expression of TRMU, GTPBP3 and MTO1 in cell models of mitochondrial-DNA diseases. Sci Rep. 2017;7(1):6209. doi: 10.1038/s41598-017-06553-w.
14. Meseguer S, Martinez-Zamora A, Garcia-Arumi E, Andreu AL, Armengod ME. The ROS-sensitive microRNA-9/9* controls the expression of mitochondrial tRNA-modifying enzymes and is involved in the molecular mechanism of MELAS syndrome. Hum Mol Genet. 2015;24(1):167-184. doi: 10.1093/hmg/ddu427.
15. Vendramin R, Marine JC, Leucci E. Non-coding RNAs: the dark side of nuclear-mitochondrial communication. EMBO J. 2017;36(9):1123-1133. doi: 10.15252/embj.201695546.
16. Wang W, Zhuang Q, Ji K, Wen B, Lin P, Zhao Y, et al. Identification of miRNA, lncRNA and mRNA-associated ceRNA networks and potential biomarker for MELAS with mitochondrial DNA A3243G mutation. Sci Rep. 2017;7:41639. doi: 10.1038/srep41639.

17. He L, Hannon GJ. MicroRNAs: small RNAs with a big role in gene regulation. Nat Rev Genet. 2004;5(7):522-531. doi: 10.1038/nrg1379.
18. Wahid F, Shehzad A, Khan T, Kim YY. MicroRNAs: synthesis, mechanism, function, and recent clinical trials. Biochim Biophys Acta. 2010;1803(11):1231-1243. doi: 10.1016/j.bbamcr.2010.06.013.
19. Paul P, Chakraborty A, Sarkar D, Langthasa M, Rahman M, Bari M, et al. Interplay between miRNAs and human diseases. J Cell Physiol. 2018;233(3):2007-2018. doi: 10.1002/jcp.25854.
20. DiMauro S, Hirano M. Melas. In: Pagon RA, Adam MP, Ardinger HH, Wallace SE, Amemiya A, Bean LJH, et al., editors. GeneReviews(R). Seattle (WA)1993.
21. El-Hattab AW, Adesina AM, Jones J, Scaglia F. MELAS syndrome: Clinical manifestations, pathogenesis, and treatment options. Mol Genet Metab. 2015;116(1-2):4-12. doi: 10.1016/j.ymgme.2015.06.004.
22. Bates MG, Bourke JP, Giordano C, d'Amati G, Turnbull DM, Taylor RW. Cardiac involvement in mitochondrial DNA disease: clinical spectrum, diagnosis, and management. Eur Heart J. 2012;33(24):3023-3033. doi: 10.1093/eurheartj/ehs275.
23. Majamaa-Voltti K, Peuhkurinen K, Kortelainen ML, Hassinen IE, Majamaa K. Cardiac abnormalities in patients with mitochondrial DNA mutation 3243A>G. BMC Cardiovasc Disord. 2002;2:12.
24. Elliott HR, Samuels DC, Eden JA, Relton CL, Chinnery PF. Pathogenic mitochondrial DNA mutations are common in the general population. Am J Hum Genet. 2008;83(2):254-260. doi: 10.1016/j.ajhg.2008.07.004.
25. Gorman GS, Schaefer AM, Ng Y, Gomez N, Blakely EL, Alston CL, et al. Prevalence of nuclear and mitochondrial DNA mutations related to adult mitochondrial disease. Ann Neurol. 2015;77(5):753-759. doi: 10.1002/ana.24362.
26. Ng YS, Grady JP, Lax NZ, Bourke JP, Alston CL, Hardy SA, et al. Sudden adult death syndrome in m.3243A>G-related mitochondrial disease: an unrecognized clinical entity in young, asymptomatic adults. Eur Heart J. 2016;37(32):2552-2559. doi: 10.1093/eurheartj/ehv306.
27. DiMauro S, Schon EA. Mitochondrial DNA mutations in human disease. Am J Med Genet. 2001;106(1):18-26. doi: 10.1002/ajmg.1392.
28. Cannino G, Di Liegro CM, Rinaldi AM. Nuclear-mitochondrial interaction. Mitochondrion. 2007;7(6):359-366. doi: 10.1016/j.mito.2007.07.001.
29. Minocherhomji S, Tollefsbol TO, Singh KK. Mitochondrial regulation of epigenetics and its role in human diseases. Epigenetics. 2012;7(4):326-334. doi: 10.4161/epi.19547.
30. Stewart JB, Chinnery PF. The dynamics of mitochondrial DNA heteroplasmy: implications for human health and disease. Nat Rev Genet. 2015;16(9):530-542. doi: 10.1038/nrg3966.
31. Jiang M, Kauppila TES, Motori E, Li X, Atanassov I, Folz-Donahue K, et al. Increased Total mtDNA Copy Number Cures Male Infertility Despite Unaltered mtDNA Mutation Load. Cell Metab. 2017;26(2):429-436 e424. doi: 10.1016/j.cmet.2017.07.003.
32. Dirkx E, da Costa Martins PA, De Windt LJ. Regulation of fetal gene expression in heart failure. Biochim Biophys Acta. 2013;1832(12):2414-2424. doi: 10.1016/j.bbadis.2013.07.023.
33. Wahbi K, Bougouin W, Behin A, Stojkovic T, Becane HM, Jardel C, et al. Long-term cardiac prognosis and risk stratification in 260 adults presenting with mitochondrial diseases. Eur Heart J. 2015;36(42):2886-2893. doi: 10.1093/eurheartj/ehv307.
34. Chomyn A. Platelet-mediated transformation of human mitochondrial DNA-less cells. Methods Enzymol. 1996;264:334-339.
35. Kim DS, Jung DS, Park KH, Kim IJ, Kim CM, Lee WH, et al. Histochemical and molecular genetic study of MELAS and MERRF in Korean patients. J Korean Med Sci. 2002;17(1):103-112. doi: 10.3346/jkms.2002.17.1.103.

36. Singh R, Ellard S, Hattersley A, Harries LW. Rapid and sensitive real-time polymerase chain reaction method for detection and quantification of 3243A>G mitochondrial point mutation. J Mol Diagn. 2006;8(2):225-230. doi: 10.2353/jmoldx.2006.050067.
37. Garcia-Garcia F, Panadero J, Dopazo J, Montaner D. Integrated gene set analysis for microRNA studies. Bioinformatics. 2016;32(18):2809-2816. doi: 10.1093/bioinformatics/btw334.
38. Brown BD, Gentner B, Cantore A, Colleoni S, Amendola M, Zingale A, et al. Endogenous microRNA can be broadly exploited to regulate transgene expression according to tissue, lineage and differentiation state. Nat Biotechnol. 2007;25(12):1457-1467. doi: 10.1038/nbt1372.
39. Zhou Q, Zheng X, Chen L, Xu B, Yang X, Jiang J, et al. Smad2/3/4 Pathway Contributes to TGF-beta-Induced MiRNA-181b Expression to Promote Gastric Cancer Metastasis by Targeting Timp3. Cell Physiol Biochem. 2016;39(2):453-466. doi: 10.1159/000445638.
40. Dong Y, Jin X, Sun Z, Zhao Y, Song X. MiR-186 Inhibited Migration of NSCLC via Targeting cdc42 and Effecting EMT Process. Mol Cells. 2017;40(3):195-201. doi: 10.14348/molcells.2017.2291.
41. Li X, Wu Y, Liu A, Tang X. MiR-27b is epigenetically downregulated in tamoxifen resistant breast cancer cells due to promoter methylation and regulates tamoxifen sensitivity by targeting HMGB3. Biochem Biophys Res Commun. 2016;477(4):768-773. doi: 10.1016/j.bbrc.2016.06.133.
42. Marques FZ, Vizi D, Khammy O, Mariani JA, Kaye DM. The transcardiac gradient of cardio-microRNAs in the failing heart. Eur J Heart Fail. 2016;18(8):1000-1008. doi: 10.1002/ejhf.517.
43. Thum T, Galuppo P, Wolf C, Fiedler J, Kneitz S, van Laake LW, et al. MicroRNAs in the human heart: a clue to fetal gene reprogramming in heart failure. Circulation. 2007;116(3):258-267. doi: 10.1161/CIRCULATIONAHA.107.687947.
44. Fayssoil A. Heart diseases in mitochondrial encephalomyopathy, lactic acidosis, and stroke syndrome. Congest Heart Fail. 2009;15(6):284-287. doi: 10.1111/j.1751-7133.2009.00108.x.
45. Okajima Y, Tanabe Y, Takayanagi M, Aotsuka H. A follow up study of myocardial involvement in patients with mitochondrial encephalomyopathy, lactic acidosis, and stroke-like episodes (MELAS). Heart. 1998;80(3):292-295.
46. Scaglia F, Towbin JA, Craigen WJ, Belmont JW, Smith EO, Neish SR, et al. Clinical spectrum, morbidity, and mortality in 113 pediatric patients with mitochondrial disease. Pediatrics. 2004;114(4):925-931. doi: 10.1542/peds.2004-0718.
47. Majamaa-Voltti K, Turkka J, Kortelainen ML, Huikuri H, Majamaa K. Causes of death in pedigrees with the 3243A>G mutation in mitochondrial DNA. J Neurol Neurosurg Psychiatry. 2008;79(2):209-211. doi: 10.1136/jnnp.2007.122648.
48. Takefuji M, Kruger M, Sivaraj KK, Kaibuchi K, Offermanns S, Wettschureck N. RhoGEF12 controls cardiac remodeling by integrating G protein- and integrin-dependent signaling cascades. J Exp Med. 2013;210(4):665-673. doi: 10.1084/jem.20122126.
49. Edlund S, Landstrom M, Heldin CH, Aspenstrom P. Transforming growth factor-beta-induced mobilization of actin cytoskeleton requires signaling by small GTPases Cdc42 and RhoA. Mol Biol Cell. 2002;13(3):902-914. doi: 10.1091/mbc.01-08-0398.
50. Bhowmick NA, Ghiassi M, Bakin A, Aakre M, Lundquist CA, Engel ME, et al. Transforming growth factor-beta1 mediates epithelial to mesenchymal transdifferentiation through a RhoA-dependent mechanism. Mol Biol Cell. 2001;12(1):27-36.
51. Lamouille S, Xu J, Derynck R. Molecular mechanisms of epithelial-mesenchymal transition. Nat Rev Mol Cell Biol. 2014;15(3):178-196. doi: 10.1038/nrm3758.
52. von Gise A, Pu WT. Endocardial and epicardial epithelial to mesenchymal transitions in heart development and disease. Circ Res. 2012;110(12):1628-1645. doi: 10.1161/CIRCRESAHA.111.259960.

53. Kovacic JC, Mercader N, Torres M, Boehm M, Fuster V. Epithelial-to-mesenchymal and endothelial-to-mesenchymal transition: from cardiovascular development to disease. Circulation. 2012;125(14):1795-1808. doi: 10.1161/CIRCULATIONAHA.111.040352.
54. Dobaczewski M, Chen W, Frangogiannis NG. Transforming growth factor (TGF)-beta signaling in cardiac remodeling. J Mol Cell Cardiol. 2011;51(4):600-606. doi: 10.1016/j.yjmcc.2010.10.033.
55. Ramos-Mondragon R, Galindo CA, Avila G. Role of TGF-beta on cardiac structural and electrical remodeling. Vasc Health Risk Manag. 2008;4(6):1289-1300.
56. Xu J, Lamouille S, Derynck R. TGF-beta-induced epithelial to mesenchymal transition. Cell Res. 2009;19(2):156-172. doi: 10.1038/cr.2009.5.
57. Clerk A, Sugden PH. Small guanine nucleotide-binding proteins and myocardial hypertrophy. Circ Res. 2000;86(10):1019-1023.
58. Wrana JL. Signaling by the TGFbeta superfamily. Cold Spring Harb Perspect Biol. 2013;5(10):a011197. doi: 10.1101/cshperspect.a011197.
59. Horbelt D, Denkis A, Knaus P. A portrait of Transforming Growth Factor beta superfamily signalling: Background matters. Int J Biochem Cell Biol. 2012;44(3):469-474. doi: 10.1016/j.biocel.2011.12.013.
60. Cai CL, Liang X, Shi Y, Chu PH, Pfaff SL, Chen J, et al. Isl1 identifies a cardiac progenitor population that proliferates prior to differentiation and contributes a majority of cells to the heart. Dev Cell. 2003;5(6):877-889.
61. Kastner P, Messaddeq N, Mark M, Wendling O, Grondona JM, Ward S, et al. Vitamin A deficiency and mutations of RXRalpha, RXRbeta and RARalpha lead to early differentiation of embryonic ventricular cardiomyocytes. Development. 1997;124(23):4749-4758.
62. Niederreither K, Dolle P. Retinoic acid in development: towards an integrated view. Nat Rev Genet. 2008;9(7):541-553. doi: 10.1038/nrg2340.
63. Stefanovic S, Zaffran S. Mechanisms of retinoic acid signaling during cardiogenesis. Mech Dev. 2017;143:9-19. doi: 10.1016/j.mod.2016.12.002.
64. Wang Y, Li Y, Guo C, Lu Q, Wang W, Jia Z, et al. ISL1 and JMJD3 synergistically control cardiac differentiation of embryonic stem cells. Nucleic Acids Res. 2016;44(14):6741-6755. doi: 10.1093/nar/gkw301.
65. Jin Y, Chen Z, Liu X, Zhou X. Evaluating the microRNA targeting sites by luciferase reporter gene assay. Methods Mol Biol. 2013;936:117-127. doi: 10.1007/978-1-62703-083-0_10.
66. Schier AF. Nodal morphogens. Cold Spring Harb Perspect Biol. 2009;1(5):a003459. doi: 10.1101/cshperspect.a003459.
67. Egerman MA, Glass DJ. Signaling pathways controlling skeletal muscle mass. Crit Rev Biochem Mol Biol. 2014;49(1):59-68. doi: 10.3109/10409238.2013.857291.
68. Blanchette F, Rivard N, Rudd P, Grondin F, Attisano L, Dubois CM. Cross-talk between the p42/p44 MAP kinase and Smad pathways in transforming growth factor beta 1-induced furin gene transactivation. J Biol Chem. 2001;276(36):33986-33994. doi: 10.1074/jbc.M100093200.
69. Mendez MG, Kojima S, Goldman RD. Vimentin induces changes in cell shape, motility, and adhesion during the epithelial to mesenchymal transition. FASEB J. 2010;24(6):1838-1851. doi: 10.1096/fj.09-151639.
70. Inman GJ, Nicolas FJ, Callahan JF, Harling JD, Gaster LM, Reith AD, et al. SB-431542 is a potent and specific inhibitor of transforming growth factor-beta superfamily type I activin receptor-like kinase (ALK) receptors ALK4, ALK5, and ALK7. Mol Pharmacol. 2002;62(1):65-74.
71. Miyamoto S, Del Re DP, Xiang SY, Zhao X, Florholmen G, Brown JH. Revisited and revised: is RhoA always a villain in cardiac pathophysiology? J Cardiovasc Transl Res. 2010;3(4):330-343. doi: 10.1007/s12265-010-9192-8.

72. Kandel J, Picard M, Wallace DC, Eckmann DM. Mitochondrial DNA 3243A>G heteroplasmy is associated with changes in cytoskeletal protein expression and cell mechanics. J R Soc Interface. 2017;14(131). doi: 10.1098/rsif.2017.0071.
73. Dodou E, Verzi MP, Anderson JP, Xu SM, Black BL. Mef2c is a direct transcriptional target of ISL1 and GATA factors in the anterior heart field during mouse embryonic development. Development. 2004;131(16):3931-3942. doi: 10.1242/dev.01256.
74. Dorn T, Goedel A, Lam JT, Haas J, Tian Q, Herrmann F, et al. Direct nkx2-5 transcriptional repression of isl1 controls cardiomyocyte subtype identity. Stem Cells. 2015;33(4):1113-1129. doi: 10.1002/stem.1923.
75. Chinnery PF, Howell N, Lightowlers RN, Turnbull DM. Molecular pathology of MELAS and MERRF. The relationship between mutation load and clinical phenotypes. Brain. 1997;120 (Pt 10):1713-1721.
76. Spater D, Hansson EM, Zangi L, Chien KR. How to make a cardiomyocyte. Development. 2014;141(23):4418-4431. doi: 10.1242/dev.091538.
77. Van Vliet P, Wu SM, Zaffran S, Puceat M. Early cardiac development: a view from stem cells to embryos. Cardiovasc Res. 2012;96(3):352-362. doi: 10.1093/cvr/cvs270.
78. Mercola M, Ruiz-Lozano P, Schneider MD. Cardiac muscle regeneration: lessons from development. Genes Dev. 2011;25(4):299-309. doi: 10.1101/gad.2018411.
79. Arnold SJ, Robertson EJ. Making a commitment: cell lineage allocation and axis patterning in the early mouse embryo. Nat Rev Mol Cell Biol. 2009;10(2):91-103. doi: 10.1038/nrm2618.
80. Phillips HM, Murdoch JN, Chaudhry B, Copp AJ, Henderson DJ. Vangl2 acts via RhoA signaling to regulate polarized cell movements during development of the proximal outflow tract. Circ Res. 2005;96(3):292-299. doi: 10.1161/01.RES.0000154912.08695.88.
81. Wei L, Imanaka-Yoshida K, Wang L, Zhan S, Schneider MD, DeMayo FJ, et al. Inhibition of Rho family GTPases by Rho GDP dissociation inhibitor disrupts cardiac morphogenesis and inhibits cardiomyocyte proliferation. Development. 2002;129(7):1705-1714.
82. Cooley JR, Yatskievych TA, Antin PB. Embryonic expression of the transforming growth factor beta ligand and receptor genes in chicken. Dev Dyn. 2014;243(3):497-508. doi: 10.1002/dvdy.24085.
83. Meyers DE, Basha HI, Koenig MK. Mitochondrial cardiomyopathy: pathophysiology, diagnosis, and management. Tex Heart Inst J. 2013;40(4):385-394.
84. Akazawa H, Komuro I. Roles of cardiac transcription factors in cardiac hypertrophy. Circ Res. 2003;92(10):1079-1088. doi: 10.1161/01.RES.0000072977.86706.23.
85. Oka T, Xu J, Molkentin JD. Re-employment of developmental transcription factors in adult heart disease. Semin Cell Dev Biol. 2007;18(1):117-131. doi: 10.1016/j.semcdb.2006.11.012.
86. Kalluri R, Weinberg RA. The basics of epithelial-mesenchymal transition. J Clin Invest. 2009;119(6):1420-1428. doi: 10.1172/JCI39104.
87. Thiery JP, Acloque H, Huang RY, Nieto MA. Epithelial-mesenchymal transitions in development and disease. Cell. 2009;139(5):871-890. doi: 10.1016/j.cell.2009.11.007.
88. Thiery JP. Epithelial-mesenchymal transitions in development and pathologies. Curr Opin Cell Biol. 2003;15(6):740-746.
89. Krainock M, Toubat O, Danopoulos S, Beckham A, Warburton D, Kim R. Epicardial Epithelial-to-Mesenchymal Transition in Heart Development and Disease. J Clin Med. 2016;5(2). doi: 10.3390/jcm5020027.
90. Limongelli G, Tome-Esteban M, Dejthevaporn C, Rahman S, Hanna MG, Elliott PM. Prevalence and natural history of heart disease in adults with primary mitochondrial respiratory chain disease. Eur J Heart Fail. 2010;12(2):114-121. doi: 10.1093/eurjhf/hfp186.
91. Shi Y, Massague J. Mechanisms of TGF-beta signaling from cell membrane to the nucleus. Cell. 2003;113(6):685-700.
92. Derynck RM, K. . The TGF-beta family. Cold Spring Harbor Laboratory Press. 2007.

93. Rifkin DB. Latent transforming growth factor-beta (TGF-beta) binding proteins: orchestrators of TGF-beta availability. J Biol Chem. 2005;280(9):7409-7412. doi: 10.1074/jbc.R400029200.
94. Rahimi RA, Leof EB. TGF-beta signaling: a tale of two responses. J Cell Biochem. 2007;102(3):593-608. doi: 10.1002/jcb.21501.
95. Feng XH, Derynck R. Specificity and versatility in tgf-beta signaling through Smads. Annu Rev Cell Dev Biol. 2005;21:659-693. doi: 10.1146/annurev.cellbio.21.022404.142018.
96. Ross S, Hill CS. How the Smads regulate transcription. Int J Biochem Cell Biol. 2008;40(3):383-408. doi: 10.1016/j.biocel.2007.09.006.
97. Zhang YE. Non-Smad pathways in TGF-beta signaling. Cell Res. 2009;19(1):128-139. doi: 10.1038/cr.2008.328.
98. Pellegrin S, Mellor H. Actin stress fibres. J Cell Sci. 2007;120(Pt 20):3491-3499. doi: 10.1242/jcs.018473.
99. Tavares AL, Mercado-Pimentel ME, Runyan RB, Kitten GT. TGF beta-mediated RhoA expression is necessary for epithelial-mesenchymal transition in the embryonic chick heart. Dev Dyn. 2006;235(6):1589-1598. doi: 10.1002/dvdy.20771.
100. Kardassis D, Murphy C, Fotsis T, Moustakas A, Stournaras C. Control of transforming growth factor beta signal transduction by small GTPases. FEBS J. 2009;276(11):2947-2965. doi: 10.1111/j.1742-4658.2009.07031.x.

Figure and Table captions

Fig 1. The MELAS mutation produces an important and specific miRNA dysregulation in 143B cells. (A and B) Dendrogram and heatmap of hierarchical clustering of the total number **(A)** and the 20 selected differentially-expressed miRNAs **(B)**. miRNA expression is hierarchically clustered on the y axis, and WT and MELAS samples are hierarchically clustered on the x axis. The legend on the left indicates the miRNA represented in the corresponding row. The relative miRNA expression is depicted according to the color scale shown on the right. Red indicates up-regulation; and blue, down-regulation. **(C)** RT-qPCR analysis of the expression of 20 selected miRNAs in MELAS cybrid cells. Data are represented as fold change respect to WT values. Differences from WT values were found to be statistically significant at *p<0.05, **p<0.01, ***p<0.001. RT-qPCR data are the mean ± SD of at least three different experiments. **(D)** Correlation analysis of log_2 fold changes obtained by both techniques, small RNAseq and RT-qPCR.

Fig 2. Expression levels of miR-598-3p, -218-5p and -4775 follow an inverse correlation with the mutation load. (A and B) RT-qPCR analysis of the expression of 10 selected down-regulated **(A)** and 10 selected up-regulated **(B)** miRNAs in MELAS cybrid cells and muscle samples from 5 patients with different heteroplasmy (cohort 1). Data are expressed as fold change respect to WT values and presented in a scatter plot with the mean ± SD of all determinations. **(C)** Correlation analysis between log_2 fold changes of the 10 selected down-regulated miRNAs and heteroplasmy levels in MELAS muscle samples from the first cohort. **(D)** Correlation and linear regression between log_2 fold changes of miR-598-3p, -218-5p, -4775, -27b-3p and -186-5p, and the heteroplasmy levels in MELAS muscle samples from cohort 1. **(E)** Correlation analysis between log_2 fold changes of the 10 selected up-regulated miRNAs and heteroplasmy levels in MELAS muscle samples from cohort 1. **(F)** RT-qPCR analysis of miR-598-3p, -218-5p, -4775, -27b-3p and -186-5p in 14 MELAS muscle samples with different heteroplasmy (5 samples from cohort 1 plus 9 samples from cohort 2). Data are expressed as fold change respect to

WT values and presented in a scatter plot with the mean ± SD of all determinations. **(G)** Correlation and linear regression between log_2 fold changes of miR-598-3p, -218-5p, -4775, -27b-3p and 186-5p, and the heteroplasmy levels in the 14 MELAS muscle samples. All data are expressed as fold change respect to WT values. Differences from WT values were found to be statistically significant at *p<0.05, **p<0.01, ***p<0.001.

Fig 3. Action of miR-218-5p and miR-4775 on TGFβ superfamily signaling and expression of fetal cardiac genes. Transforming growth factor-β (TGF-β) superfamily signaling plays critical roles in embryonic development and adult tissue homeostasis through the regulation of many cellular processes including epithelial-mesenchymal transition (EMT) [91]. The TGF-β superfamily comprises 33 structurally related secreted growth factors including TGF-βs, NODAL, Activins and Bone Morphogenetic Proteins (BMPs) [92]. All TGF-β and most BMP ligands are secreted as pro-peptides in which the mature growth factor domain, generated after cleavage by a convertase (CV) such as Furin, remains non-covalently attached to the pro-domain [93]. Binding of TGF-β and BMP ligands to their receptors induces the formation of active receptor signaling complexes which phosphorylate receptor-activated Smad (R-Smad) proteins (Smad2 and Smad3 for the TGF-β/activin pathway, or Smad1/5/9 for the BMP pathway), which associate with Smad4 and accumulate in the nucleus [94]. In the nucleus, Smads regulate gene expression assisted by transcriptional co-factors, co-activators, or co-repressors [95, 96]. Moreover, TGF-β signaling can affect Smad-independent pathways, including RHO GTPase signaling [97]. RHOA activates downstream target proteins, such as ROCK1, promoting rearrangement of the actin cytoskeleton [98, 99]. Other Rho subfamily members, CDC42 and RAC1, also participate in actin reorganization following TGF-β activation [100]. This work demonstrates that miR-258-5p targets *NODAL* and *RHOA*, while miR-4775 targets *ISL1* and *RXRB*.

Fig 4. *NODAL* and *RHOA* are up-regulated in MELAS cybrids via miR-218-5p. (A) RT-qPCR analysis of *NODAL* and *RHOA* mRNA expression in MELAS cybrid cells. Data are represented as fold change respect to WT values. **(B)** Representative immunoblots of NODAL and RHOA in WT and MELAS cybrid

cells. Porin was used as a loading control. The scatter plot shows the densitometric analysis of NODAL and RHOA normalized to porin, and represented as fold change relative to WT. **(C)** RT-qPCR analysis of the *NODAL* and *RHOA* mRNA expression in pre-miR-218-5p-transfected WT cybrid cells. Data are represented as fold change relative to Negative Control (NC)-pre-miR-transfected WT cells. **(D)** Representative immunoblots of NODAL and RHOA in pre-miR-218-5p- and NC-pre-miR-transfected WT cells cybrid cells. Porin was used as a loading control. The scatter plot shows the densitometric analysis of these proteins normalized to porin and represented as fold change relative to NC-premiR-transfected WT cells. **(E)** RT-qPCR analysis of the *RHOA* mRNA expression in MELAS, and pre-miR-218-5p- and NC-pre-miR-transfected MELAS cybrid cells. Data are represented as fold change respect to WT values. **(F)** Representative immunoblots of RHOA in WT, MELAS, and pre-miR-218-5p and NC-pre-miR-transfected MELAS cybrid cells. Porin was used as a loading control. The scatter plot shows the densitometric analysis of these proteins normalized to porin and represented as fold change respect to WT values. **(G)** Effects of miR-218-5p transfection on the activity of luciferase reporter constructs containing the RHOA-3'-UTR or NODAL-3'-UTR in the direct (+) or reverse (-) direction. All data are the mean ± SD of at least three different experiments. Differences from WT values were found to be statistically significant at *p<0.05, **p<0.01, ***p<0.001.

Fig 5. *ISL1* and *RXRB* are up-regulated in MELAS cybrids via miR-4775. **(A)** RT-qPCR analysis of *ISL1* and *RXRB* mRNA expression in MELAS cybrid cells. Data are represented as fold change respect to WT values. **(B)** Representative immunoblots of ISL1 and RXRB. The scatter plot shows the densitometric analysis of ISL1 and RXRB normalized to porin and represented as fold change relative to WT. **(C)** RT-qPCR analysis of the *ISL1* and *RXRB* mRNA expression in pre-miR-4775-transfected WT cybrid cells. Data are represented as fold change relative to NC-pre-miR-transfected WT cells. **(D)** Representative immunoblots of ISL1 and RXRB in pre-miR-4775- and NC-pre-miR-transfected WT cells. Porin was used as a loading control. The scatter plot shows the densitometric analysis of these proteins normalized to porin and represented as fold change relative to NC-premiR-transfected WT cells. **(E)** RT-

qPCR analysis of the *ISL1* and *RXRB* mRNA expression in MELAS, and pre-miR-4775- and NC-pre-miR-transfected MELAS cybrid cells. Data are represented as fold change relative to WT cells **(F)** Representative immunoblots of ISL1 and RXRB in WT, MELAS, and pre-miR-4775- and NC-pre-miR-transfected MELAS cybrid cells. Porin was used as a loading control. The scatter plot shows the densitometric analysis of these proteins normalized to porin and represented as fold change relative to WT cells. **(G)** Effects of miR-4775 transfection on the activity of luciferase reporter constructs containing the ISL1-3'-UTR or RXRB-3'-UTR in the direct (+) or reverse (-) direction. Data are represented as fold change relative to WT cells. All data are the mean ± SD of at least three different experiments. Differences from WT values were found to be statistically significant at *p<0.05, **p<0.01, ***p<0.001.

Fig 6. TGF-β signaling pathway and an EMT-like program are activated in MELAS cybrid cells. (A) RT-qPCR analysis of *TGF-β3*, *MSTN, BMP4, Lefty1 and Lefty2* mRNA expression in MELAS cybrid cells. Data are represented as fold change respect to WT values. **(B)** Representative immunoblots of TGF-β signaling elements (Furin, TGF-β3, TβR-II, ActR-IIb, phosphor-Smad2 and 3, Smad2 and 3, SNAI1, ROCK1 and Rac1) in WT and MELAS cybrid cells. Porin was used as a loading control. The scatter plot shows the densitometric analysis of TGF-β signaling elements normalized to porin and represented as fold change relative to WT. **(C)** The scatter plot shows the densitometric analysis of phosphor-Smad2/3 normalized to Smad2/3 and represented as fold change relative to WT. **(D)** RT-qPCR analysis of Vimentin, E-cadherin and N-cadherin mRNA expression in MELAS cybrid cells. Data are represented as fold change respect to WT values. **(E)** Representative immunoblots of Vimentin and E-cadherin in WT and MELAS cybrid cells. Porin was used as a loading control. The scatter plot shows the densitometric analysis of Vimentin and E-cadherin normalized to porin, and represented as fold change relative to WT. **(F)** Representative images of rhodamine-phalloidin staining for F-actin (red) and DAPI for cell nucleus (blue) of WT and MELAS cybrid cells treated or not with 30 μM of the TGF-β inhibitor SB-431542 for 24h. Stress fibers are indicated with a white arrow. Scale bar, 50 μm. **(G)** Quantification of the percentage of WT and MELAS cybrid cells, treated or not with the TGF-β inhibitor SB-431542,

that show stress fibers. At least 350 cells were quantified per condition and per experiment. All data are the mean ± SD of at least three different experiments. Differences from WT values were found to be statistically significant at *p<0.05, **p<0.01, ***p<0.001.

Fig 7. Inhibition of TGF-β signaling or increasing levels of miR-4775 revert MELAS phenotypic traits. (A) Representative immunoblots of phosphor-Smad2 and 3, Smad2 and 3, and SNAI1 in MELAS cybrid cells treated or not with 30 μM of the TGF-β inhibitor SB-431542 for 24h. Porin was used as a loading control. The scatter plot shows the ratio of phosphor-Smad2/3 versus Smad2/3 and SNAI1 versus porin in treated or untreated MELAS cybrids represented as fold change relative to WT. **(B)** Representative immunoblots of SNAI1 in WT, MELAS, and pre-miR-218-5p- and NC-pre-miR-transfected MELAS cybrid cells. Porin was used as a loading control. The scatter plot shows the densitometric analysis of this protein normalized to porin and represented as fold change relative to WT cybrid cells. **(C)** RT-qPCR analysis of mRNA expression of the ISL1-targets *MEF2C* and *TNNT2* in MELAS, and pre-miR-4775- and NC-pre-miR-transfected MELAS cybrid cells. All data are the mean ± SD of at least three different experiments. Differences from WT values were found to be statistically significant at *p<0.05 and **p<0.01.

Fig 8. Anti-correlative expression between miR-4775 and miR-218-5p and their respective targets in MELAS muscle samples. (A and B) RT-qPCR analysis of the *NODAL*, *RHOA* **(A)**, *ISL1*, *MEF2c* (ISL1 target) and *RXRB* **(B)** mRNA expression in several MELAS muscle samples from cohort 1 **(B)** and cohort 2 **(A)**. **(C)** Comparison between the $\log_2$ fold changes of miRNA-218-5p and -4775, and their respective targets. Data from the same sample are circled. Samples with heteroplasmy levels higher than 60% are inside the rectangle. All data are represented as fold change respect to control values.

Table 1. Classification of MELAS and WT-derived sequences in non-coding RNA classes according to GRCh.38.ncrna. ***p<0.001

Table 1.

small RNA sequences	WT	MELAS
lincRNA	253436,7 (1,75%)	332119,3 (2,80%)
processed transcript	3280,7 (0,023%)	4455,7 (0,038%)
antisense	68920,3 (0,48%)	90904,7 (0,77%)
retained intron	10393,3 (0,072%)	8974,7 (0,076%)
sense overlapping	2005,7 (0,014%)	2445,3 (0,021%)
sense intronic	20590,7 (0,14%)	19298,7 (0,16%)
snRNA	34819 (0,24%)	51047 (0,43%)
miscRNA	46710,7 (0,32%)	36894 (0,31%)
rRNA	3314 (0,023%)	3511,3 (0,03%)
snoRNA	508103 (3,52%)	574568,7 (4,84%)
mt-tRNA	130212,3 (0,9%)	164742,3 (1,39%)
mt-rRNA	108891,7 (0,75%)	112350,7 (0,95%)
pseudogene	3,3 (0,000023%)	2,7 (0,000023%)
3'overlapping ncrna	491,3 (0,0034%)	689,3 (0,0058%)
miRNA***	13263180 (91,76%)	10469540 (88,19%)
Total sequences	14454352 (100%)	11871544 (100%)

Highlights

- The MELAS mutation m.3243A>G triggers an important miRNA response in 143B cells.
- Expression of certain miRNAs declines with high mutation heteroplasmy in muscle.
- m.3243A>G promotes reactivation of pathological cardiac remodeling genes via miRNAs
- Low levels of certain miRNAs may be a risk marker of MELAS cardiomyopathy.

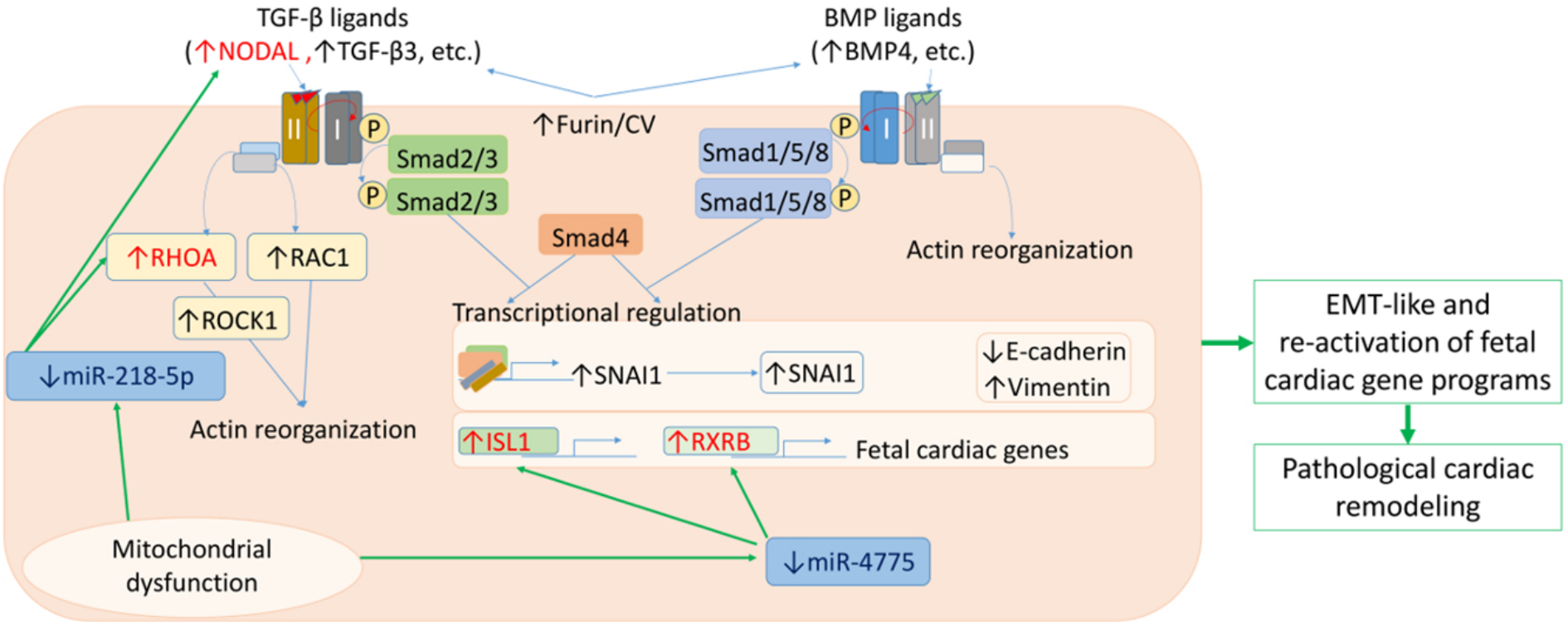

Graphics Abstract

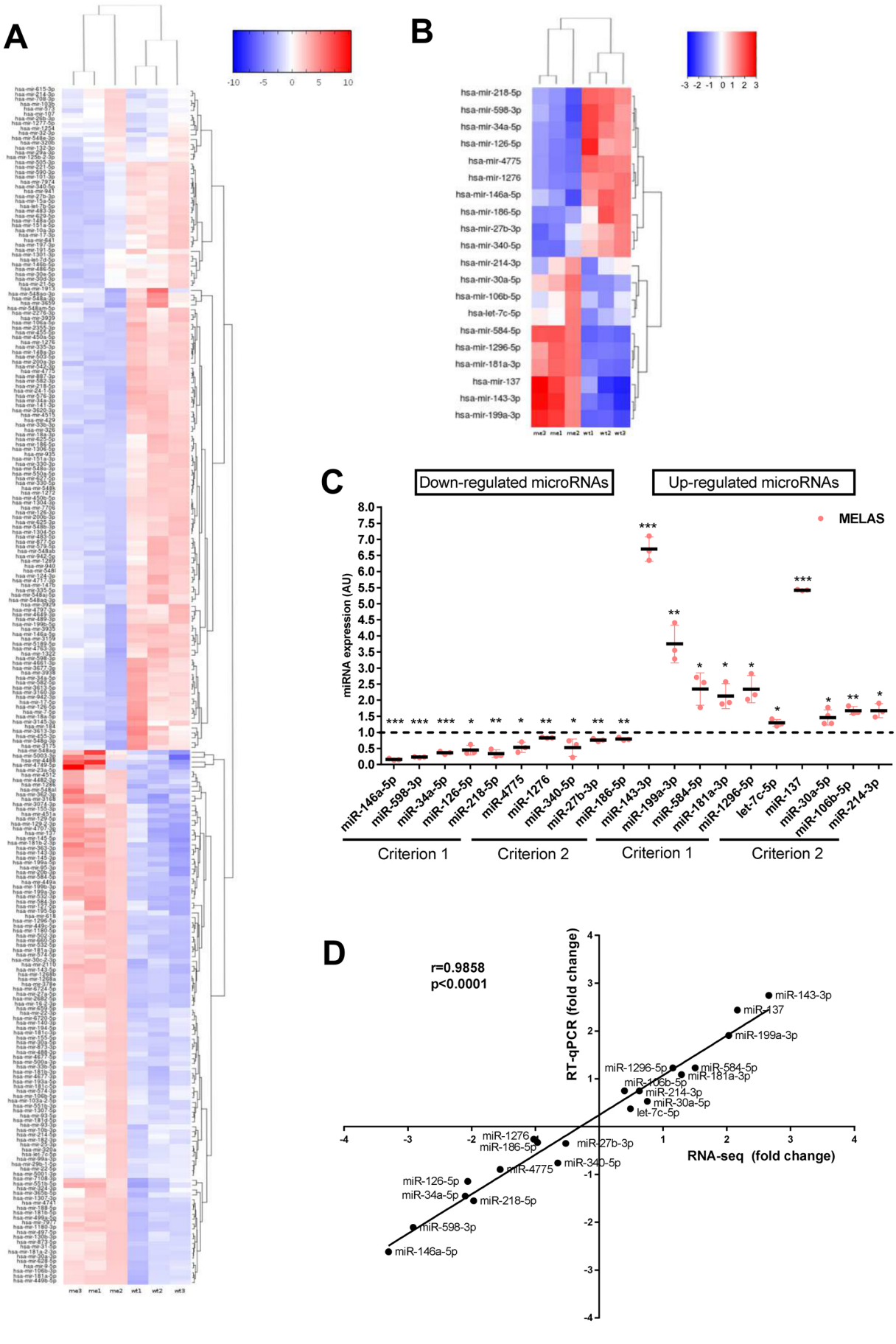
A
-10 -5 0 5 10
mre3 mre1 mre2 wt1 wt2 wt3
B
-3 -2 -1 0 1 2 3
hsa-mir-218-5p
hsa-mir-598-3p
hsa-mir-34a-5p
hsa-mir-126-5p
hsa-mir-4775
hsa-mir-1276
hsa-mir-146a-5p
hsa-mir-186-5p
hsa-mir-27b-3p
hsa-mir-340-5p
hsa-mir-214-3p
hsa-mir-30a-5p
hsa-mir-106b-5p
hsa-let-7c-5p
hsa-mir-584-5p
hsa-mir-1296-5p
hsa-mir-181a-3p
hsa-mir-137
hsa-mir-143-3p
hsa-mir-199a-3p
mre3 mre1 mre2 wt1 wt2 wt3
C
Down-regulated microRNAs
Up-regulated microRNAs
MELAS
miRNA expression (AU)
8.0
7.5
7.0
6.5
6.0
5.5
5.0
4.5
4.0
3.5
3.0
2.5
2.0
1.5
1.0
0.5
0.0
miR-146a-5p
miR-598-3p
miR-34a-5p
miR-126-5p
miR-218-5p
miR-4775
miR-1276
miR-340-5p
miR-27b-3p
miR-186-5p
miR-143-3p
miR-199a-3p
miR-584-5p
miR-181a-3p
miR-1296-5p
let-7c-5p
miR-137
miR-30a-5p
miR-106b-5p
miR-214-3p
Criterion 1
Criterion 2
Criterion 1
Criterion 2
D
r=0.9858
p<0.0001
RT-qPCR (fold change)
RNA-seq (fold change)
miR-143-3p
miR-137
miR-199a-3p
miR-1296-5p
miR-584-5p
miR-181a-3p
miR-106b-5p
miR-214-3p
miR-30a-5p
let-7c-5p
miR-1276
miR-186-5p
miR-27b-3p
miR-340-5p
miR-4775
miR-126-5p
miR-34a-5p
miR-218-5p
miR-598-3p
miR-146a-5p

Figure 1

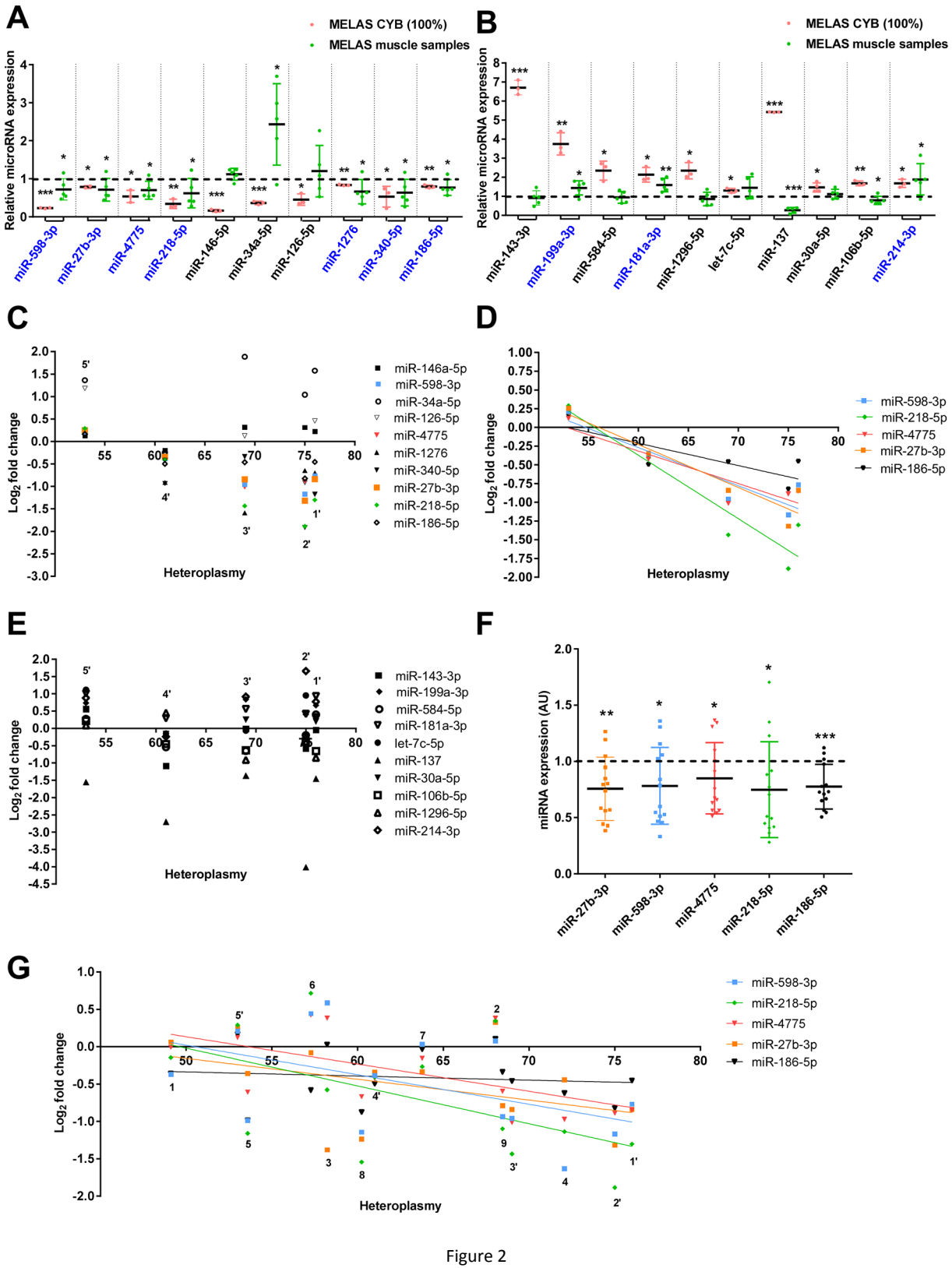
A
MELAS CYB (100%)
MELAS muscle samples
Relative microRNA expression
miR-598-3p
miR-27b-3p
miR-4775
miR-218-5p
miR-146-5p
miR-34a-5p
miR-126-5p
miR-1276
miR-340-5p
miR-186-5p
B
MELAS CYB (100%)
MELAS muscle samples
Relative microRNA expression
miR-143-3p
miR-199a-3p
miR-584-5p
miR-181a-3p
miR-1296-5p
let-7c-5p
miR-137
miR-30a-5p
miR-106b-5p
miR-214-3p
C
Log2 fold change
Heteroplasmy
miR-146a-5p
miR-598-3p
miR-34a-5p
miR-126-5p
miR-4775
miR-1276
miR-340-5p
miR-27b-3p
miR-218-5p
miR-186-5p
D
Log2 fold change
Heteroplasmy
miR-598-3p
miR-218-5p
miR-4775
miR-27b-3p
miR-186-5p
E
Log2 fold change
Heteroplasmy
miR-143-3p
miR-199a-3p
miR-584-5p
miR-181a-3p
let-7c-5p
miR-137
miR-30a-5p
miR-106b-5p
miR-1296-5p
miR-214-3p
F
miRNA expression (AU)
miR-27b-3p
miR-598-3p
miR-4775
miR-218-5p
miR-186-5p
G
Log2 fold change
Heteroplasmy
miR-598-3p
miR-218-5p
miR-4775
miR-27b-3p
miR-186-5p

Figure 2

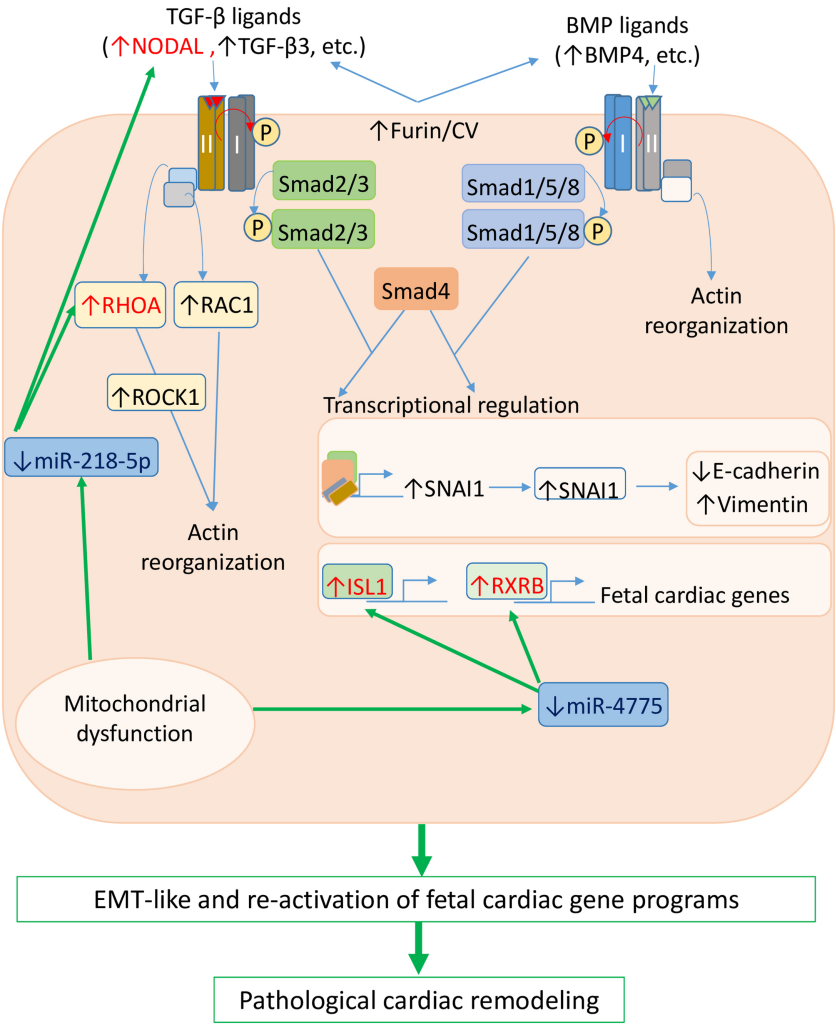
TGF-β ligands
(↑NODAL , ↑TGF-β3, etc.)
BMP ligands
(↑BMP4, etc.)
↑Furin/CV
P
Smad2/3
Smad2/3
Smad1/5/8
Smad1/5/8
Smad4
↑RHOA
↑RAC1
↑ROCK1
Actin reorganization
Actin reorganization
Transcriptional regulation
↑SNAI1
↑SNAI1
↓E-cadherin
↑Vimentin
↑ISL1
↑RXRB
Fetal cardiac genes
↓miR-218-5p
↓miR-4775
Mitochondrial dysfunction
EMT-like and re-activation of fetal cardiac gene programs
Pathological cardiac remodeling

Figure 3

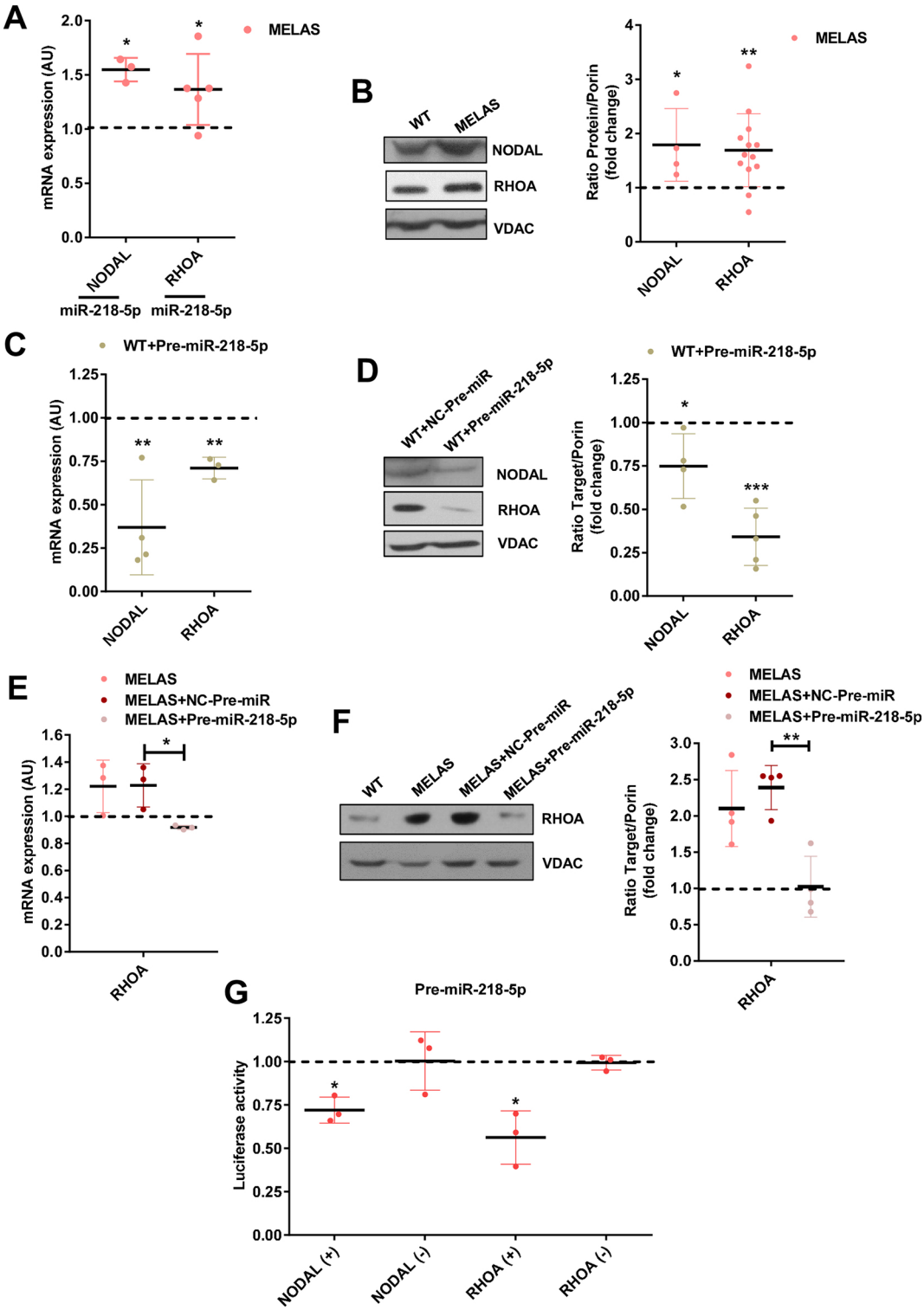
A
MELAS
mRNA expression (AU)
2.0
1.5
1.0
0.5
0.0
*
*
NODAL
RHOA
miR-218-5p
miR-218-5p
B
WT
MELAS
NODAL
RHOA
VDAC
MELAS
Ratio Protein/Porin (fold change)
4
3
2
1
0
*
**
NODAL
RHOA
C
WT+Pre-miR-218-5p
mRNA expression (AU)
1.25
1.00
0.75
0.50
0.25
0.00
**
**
NODAL
RHOA
D
WT+NC-Pre-miR
WT+Pre-miR-218-5p
NODAL
RHOA
VDAC
WT+Pre-miR-218-5p
Ratio Target/Porin (fold change)
1.25
1.00
0.75
0.50
0.25
0.00
*
***
NODAL
RHOA
E
MELAS
MELAS+NC-Pre-miR
MELAS+Pre-miR-218-5p
mRNA expression (AU)
1.6
1.4
1.2
1.0
0.8
0.6
0.4
0.2
0.0
*
RHOA
F
WT
MELAS
MELAS+NC-Pre-miR
MELAS+Pre-miR-218-5p
RHOA
VDAC
MELAS
MELAS+NC-Pre-miR
MELAS+Pre-miR-218-5p
Ratio Target/Porin (fold change)
3.0
2.5
2.0
1.5
1.0
0.5
0.0
**
RHOA
G
Pre-miR-218-5p
Luciferase activity
1.25
1.00
0.75
0.50
0.25
0.00
*
*
NODAL (+)
NODAL (-)
RHOA (+)
RHOA (-)

Figure 4

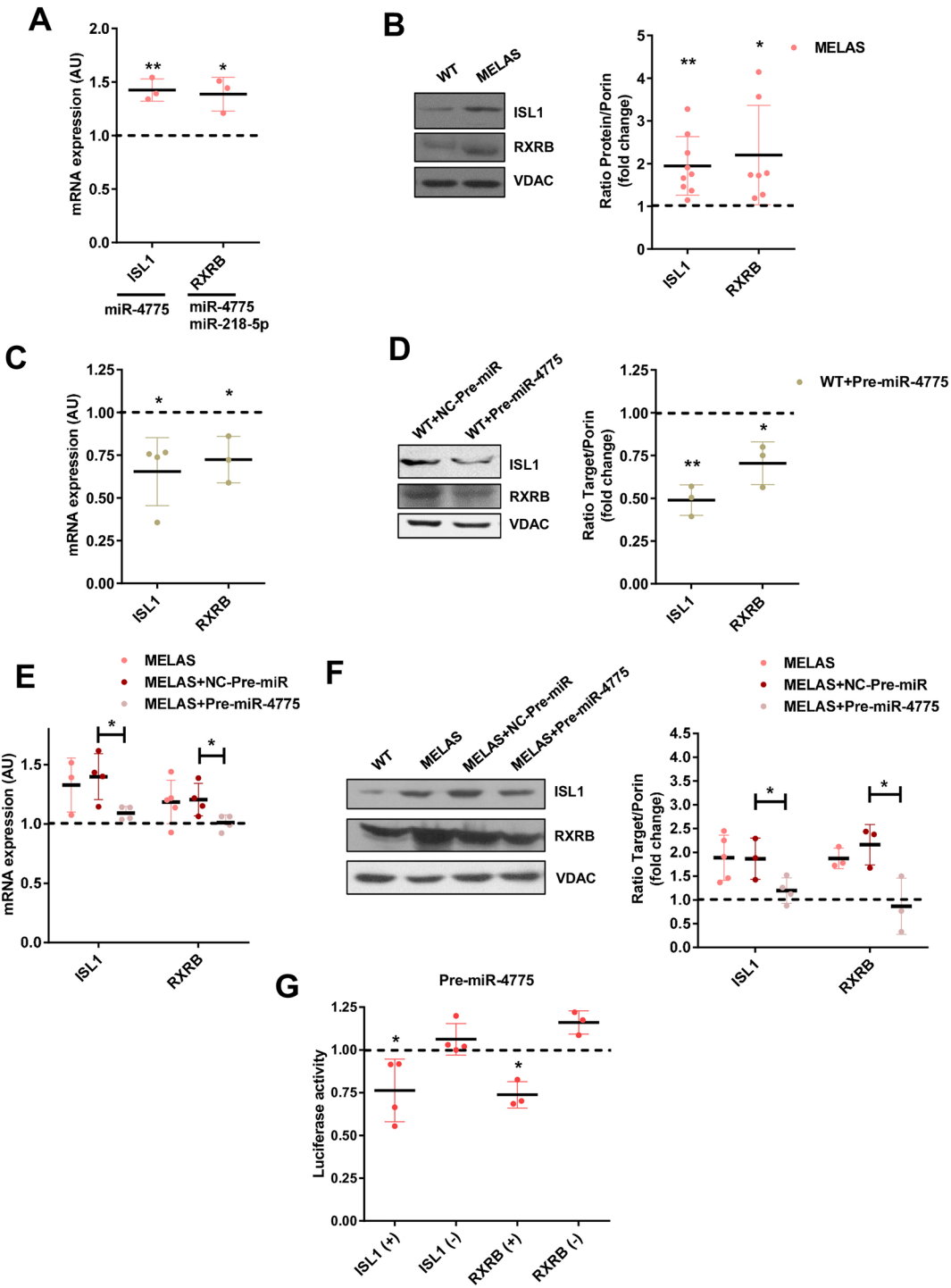
A
mRNA expression (AU)
ISL1
RXRB
miR-4775
miR-4775
miR-218-5p
B
WT
MELAS
ISL1
RXRB
VDAC
Ratio Protein/Porin
(fold change)
MELAS
C
mRNA expression (AU)
D
WT+NC-Pre-miR
WT+Pre-miR-4775
Ratio Target/Porin
(fold change)
E
MELAS
MELAS+NC-Pre-miR
MELAS+Pre-miR-4775
F
G
Pre-miR-4775
Luciferase activity
ISL1 (+)
ISL1 (-)
RXRB (+)
RXRB (-)

Figure 5

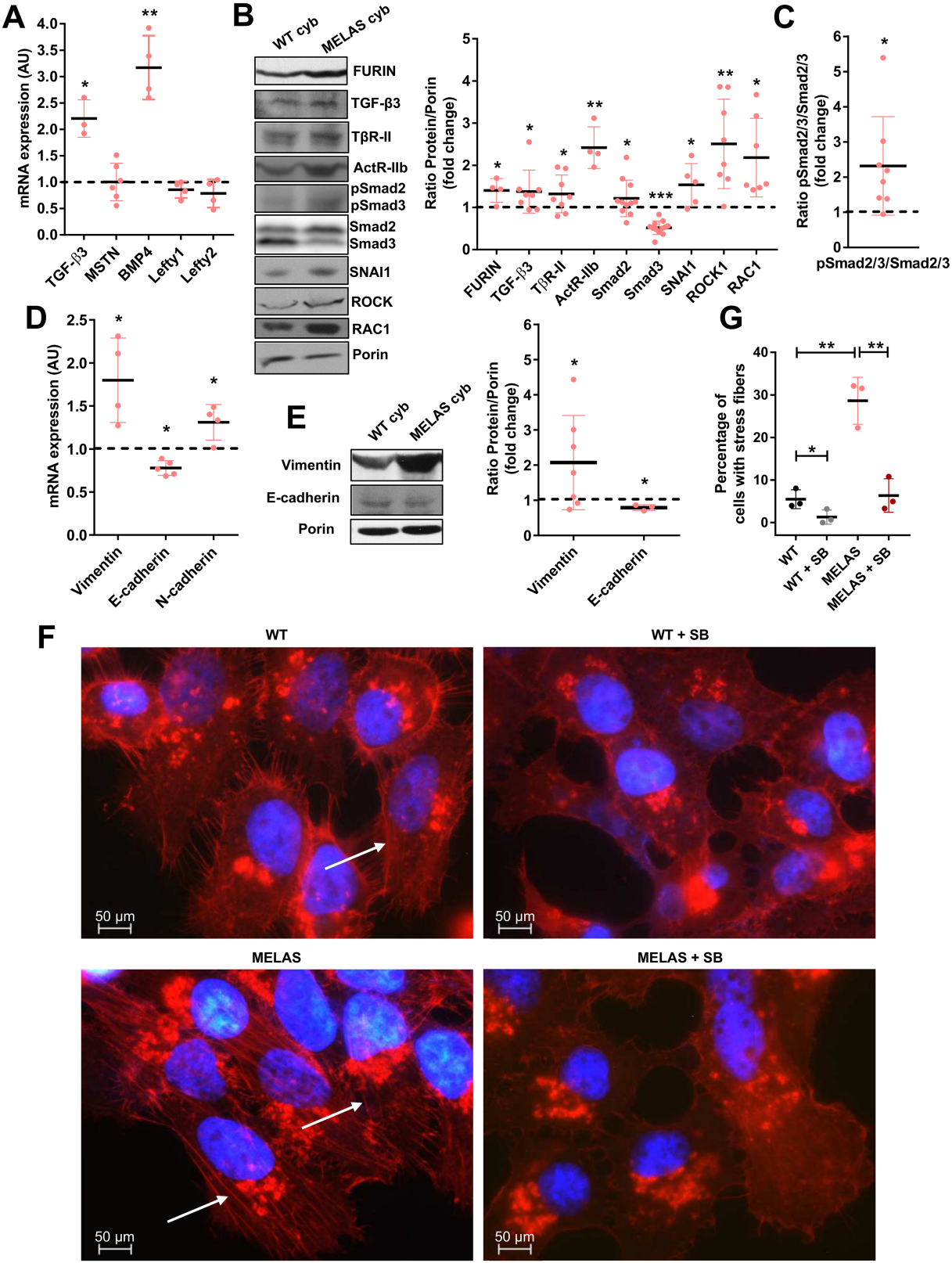
A
mRNA expression (AU)
TGF-β3
MSTN
BMP4
Lefty1
Lefty2
B
WT cyb
MELAS cyb
FURIN
TGF-β3
TβR-II
ActR-IIb
pSmad2
pSmad3
Smad2
Smad3
SNAI1
ROCK
RAC1
Porin
Ratio Protein/Porin (fold change)
C
Ratio pSmad2/3/Smad2/3 (fold change)
pSmad2/3/Smad2/3
D
mRNA expression (AU)
Vimentin
E-cadherin
N-cadherin
E
WT cyb
MELAS cyb
Vimentin
E-cadherin
Porin
Ratio Protein/Porin (fold change)
G
Percentage of cells with stress fibers
WT
WT + SB
MELAS
MELAS + SB
F
WT
WT + SB
MELAS
MELAS + SB
50 µm

Figure 6

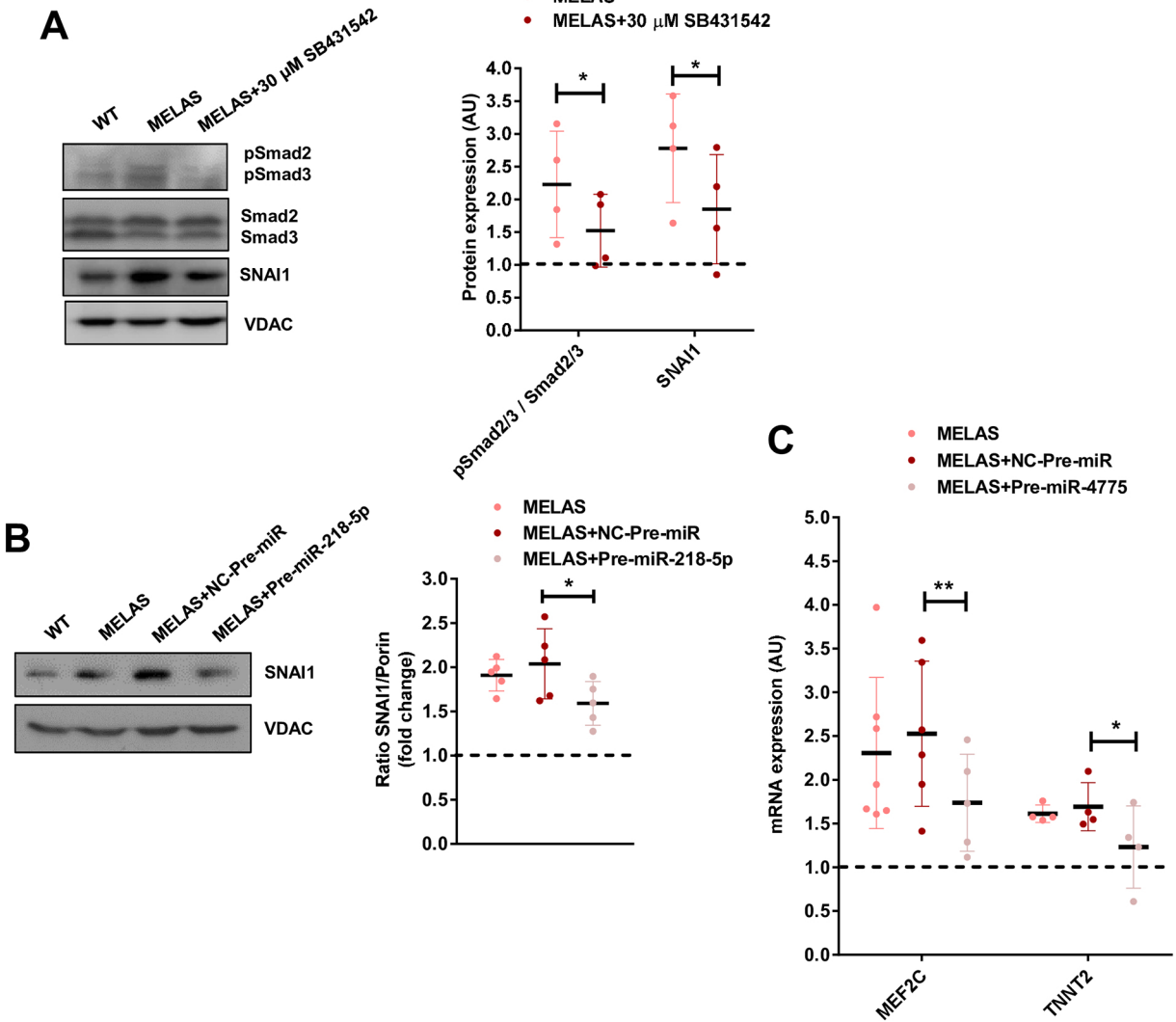
A
WT
MELAS
MELAS+30 μM SB431542
pSmad2
pSmad3
Smad2
Smad3
SNAI1
VDAC
MELAS
MELAS+30 μM SB431542
Protein expression (AU)
4.0
3.5
3.0
2.5
2.0
1.5
1.0
0.5
0.0
*
*
pSmad2/3 / Smad2/3
SNAI1
B
WT
MELAS
MELAS+NC-Pre-miR
MELAS+Pre-miR-218-5p
SNAI1
VDAC
MELAS
MELAS+NC-Pre-miR
MELAS+Pre-miR-218-5p
Ratio SNAI1/Porin
(fold change)
3.0
2.5
2.0
1.5
1.0
0.5
0.0
*
C
MELAS
MELAS+NC-Pre-miR
MELAS+Pre-miR-4775
mRNA expression (AU)
5.0
4.5
4.0
3.5
3.0
2.5
2.0
1.5
1.0
0.5
0.0
**
*
MEF2C
TNNT2

Figure 7

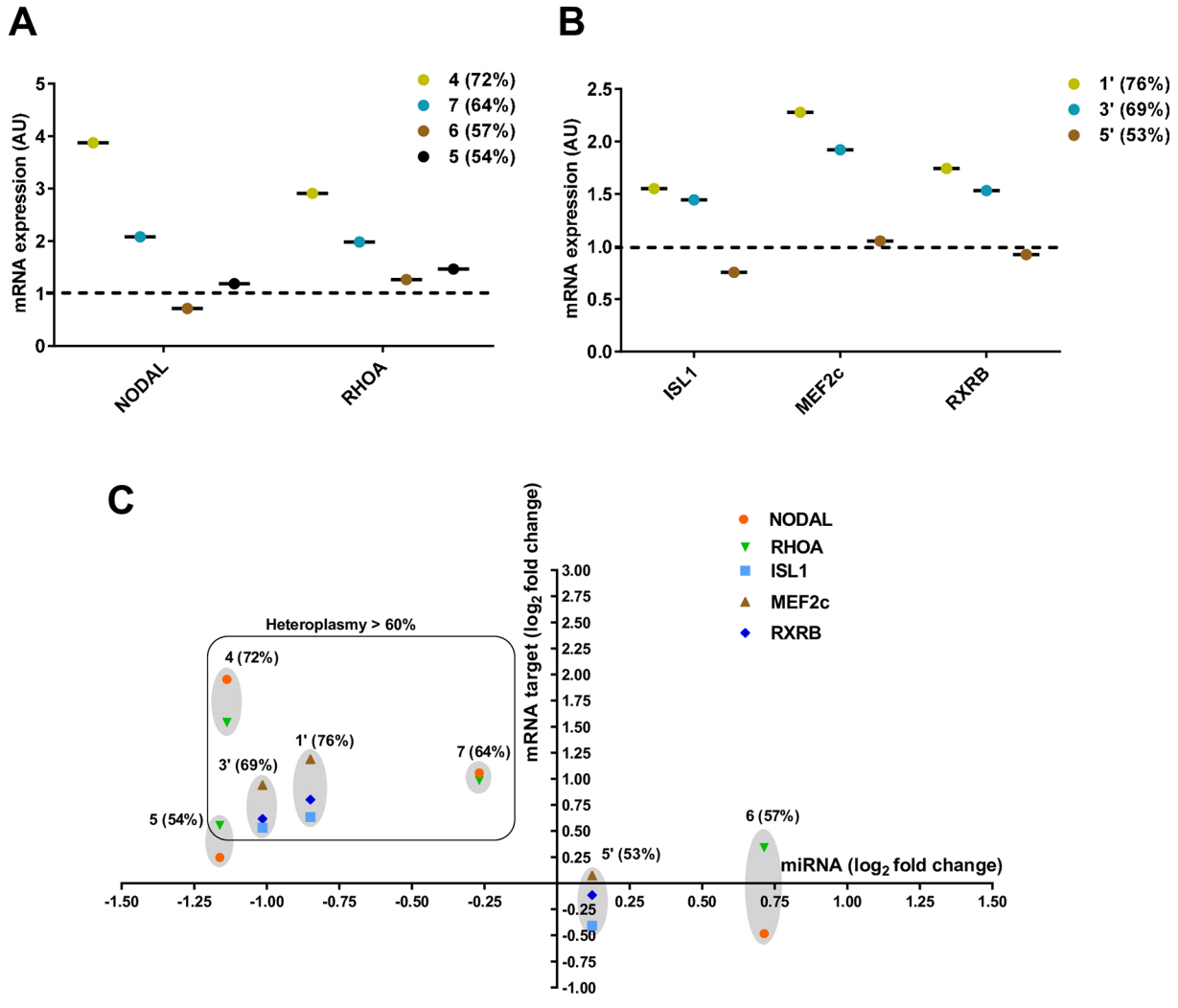
A
mRNA expression (AU)
4 (72%)
7 (64%)
6 (57%)
5 (54%)
NODAL
RHOA
B
mRNA expression (AU)
1' (76%)
3' (69%)
5' (53%)
ISL1
MEF2c
RXRB
C
mRNA target (log2 fold change)
miRNA (log2 fold change)
NODAL
RHOA
ISL1
MEF2c
RXRB
Heteroplasmy > 60%
4 (72%)
1' (76%)
3' (69%)
7 (64%)
5 (54%)
6 (57%)
5' (53%)

Figure 8

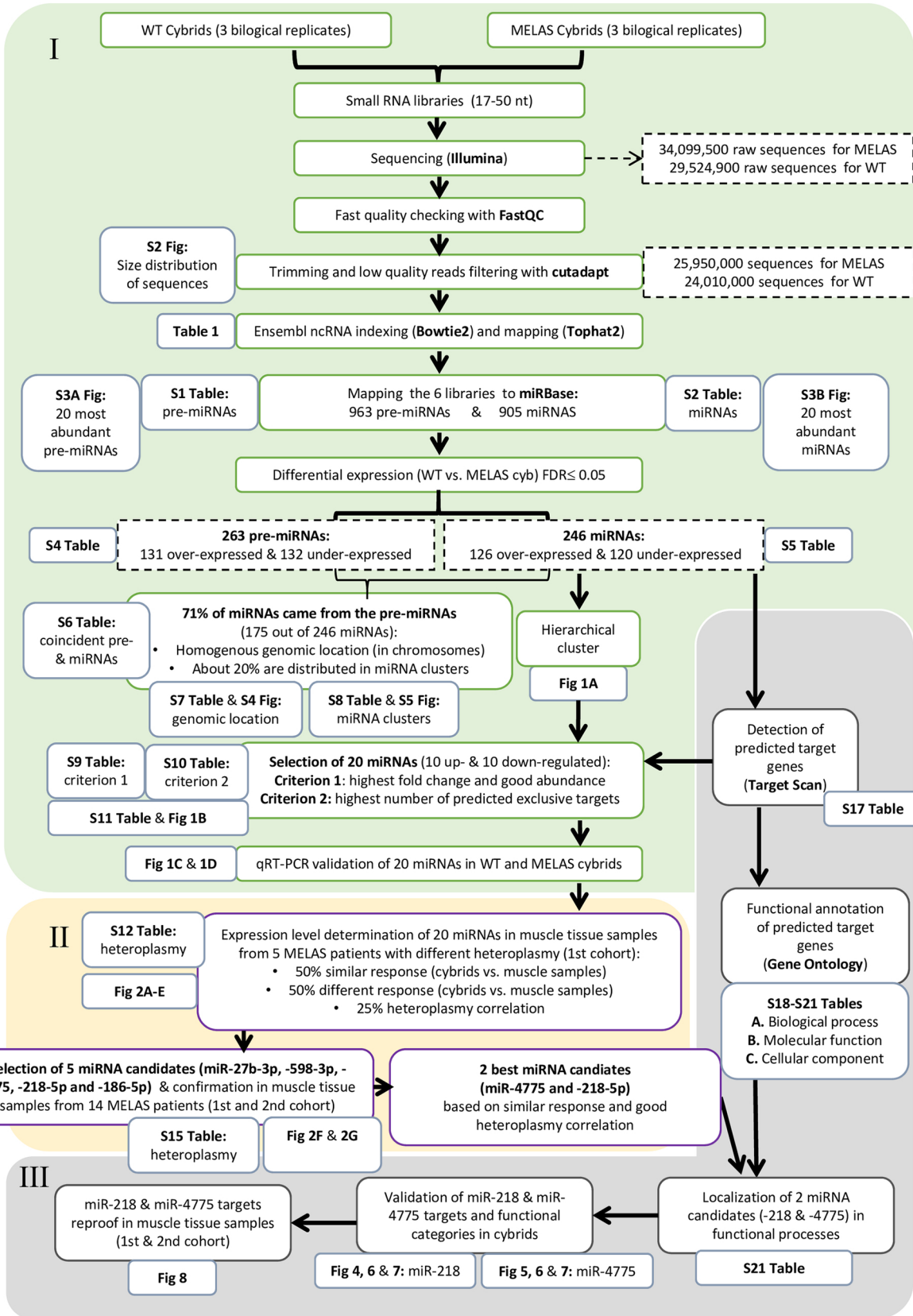
I
WT Cybrids (3 bilogical replicates)
MELAS Cybrids (3 bilogical replicates)
Small RNA libraries (17-50 nt)
Sequencing (Illumina)
34,099,500 raw sequences for MELAS
29,524,900 raw sequences for WT
Fast quality checking with FastQC
S2 Fig: Size distribution of sequences
Trimming and low quality reads filtering with cutadapt
25,950,000 sequences for MELAS
24,010,000 sequences for WT
Table 1
Ensembl ncRNA indexing (Bowtie2) and mapping (Tophat2)
S3A Fig: 20 most abundant pre-miRNAs
S1 Table: pre-miRNAs
Mapping the 6 libraries to miRBase: 963 pre-miRNAs & 905 miRNAS
S2 Table: miRNAs
S3B Fig: 20 most abundant miRNAs
Differential expression (WT vs. MELAS cyb) FDR≤ 0.05
S4 Table
263 pre-miRNAs: 131 over-expressed & 132 under-expressed
246 miRNAs: 126 over-expressed & 120 under-expressed
S5 Table
S6 Table: coincident pre- & miRNAs
71% of miRNAs came from the pre-miRNAs (175 out of 246 miRNAs):
• Homogenous genomic location (in chromosomes)
• About 20% are distributed in miRNA clusters
S7 Table & S4 Fig: genomic location
S8 Table & S5 Fig: miRNA clusters
Hierarchical cluster
Fig 1A
S9 Table: criterion 1
S10 Table: criterion 2
S11 Table & Fig 1B
Selection of 20 miRNAs (10 up- & 10 down-regulated):
Criterion 1: highest fold change and good abundance
Criterion 2: highest number of predicted exclusive targets
Detection of predicted target genes (Target Scan)
S17 Table
Fig 1C & 1D
qRT-PCR validation of 20 miRNAs in WT and MELAS cybrids
II
S12 Table: heteroplasmy
Fig 2A-E
Expression level determination of 20 miRNAs in muscle tissue samples from 5 MELAS patients with different heteroplasmy (1st cohort):
• 50% similar response (cybrids vs. muscle samples)
• 50% different response (cybrids vs. muscle samples)
• 25% heteroplasmy correlation
Functional annotation of predicted target genes (Gene Ontology)
S18-S21 Tables
A. Biological process
B. Molecular function
C. Cellular component
Selection of 5 miRNA candidates (miR-27b-3p, -598-3p, -4775, -218-5p and -186-5p) & confirmation in muscle tissue samples from 14 MELAS patients (1st and 2nd cohort)
S15 Table: heteroplasmy
Fig 2F & 2G
2 best miRNA candiates (miR-4775 and -218-5p) based on similar response and good heteroplasmy correlation
III
miR-218 & miR-4775 targets reproof in muscle tissue samples (1st & 2nd cohort)
Fig 8
Validation of miR-218 & miR-4775 targets and functional categories in cybrids
Fig 4, 6 & 7: miR-218
Fig 5, 6 & 7: miR-4775
Localization of 2 miRNA candidates (-218 & -4775) in functional processes
S21 Table

Figure 9

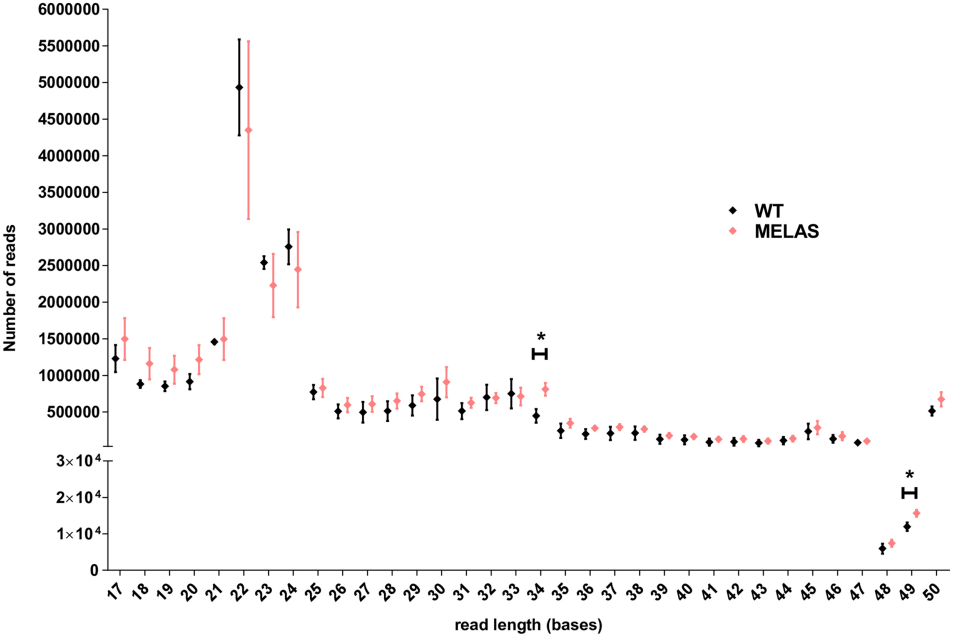
6000000
5500000
5000000
4500000
4000000
3500000
3000000
2500000
2000000
1500000
1000000
500000
3×10⁴
2×10⁴
1×10⁴
0
Number of reads
WT
MELAS
*
*
17 18 19 20 21 22 23 24 25 26 27 28 29 30 31 32 33 34 35 36 37 38 39 40 41 42 43 44 45 46 47 48 49 50
read length (bases)

Figure 10

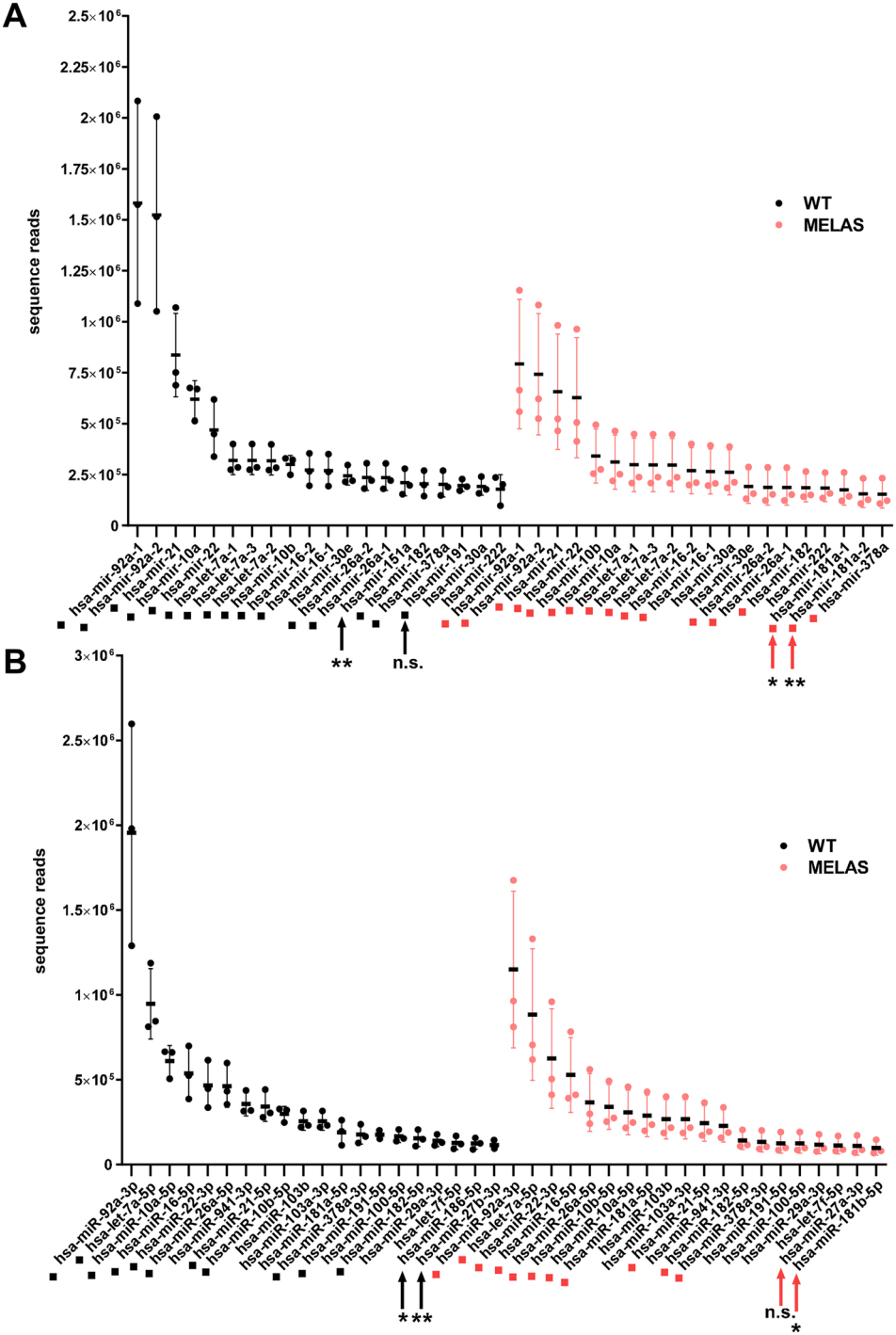
A
sequence reads
2.5×10^6
2.25×10^6
2×10^6
1.75×10^6
1.5×10^6
1.25×10^6
1×10^6
7.5×10^5
5×10^5
2.5×10^5
0
WT
MELAS
hsa-mir-92a-1
hsa-mir-92a-2
hsa-mir-21
hsa-mir-10a
hsa-mir-22
hsa-let-7a-1
hsa-let-7a-3
hsa-let-7a-2
hsa-mir-10b
hsa-mir-16-2
hsa-mir-16-1
hsa-mir-30e
hsa-mir-26a-2
hsa-mir-26a-1
hsa-mir-151a
hsa-mir-182
hsa-mir-378a
hsa-mir-191
hsa-mir-30a
hsa-mir-222
hsa-mir-92a-1
hsa-mir-92a-2
hsa-mir-21
hsa-mir-22
hsa-mir-10b
hsa-mir-10a
hsa-let-7a-1
hsa-let-7a-3
hsa-let-7a-2
hsa-mir-16-2
hsa-mir-16-1
hsa-mir-30a
hsa-mir-30e
hsa-mir-25a-2
hsa-mir-26a-1
hsa-mir-182
hsa-mir-222
hsa-mir-181a-1
hsa-mir-181a-2
hsa-mir-378a
**
n.s.
* **
B
sequence reads
3×10^6
2.5×10^6
2×10^6
1.5×10^6
1×10^6
5×10^5
0
WT
MELAS
hsa-miR-92a-3p
hsa-let-7d-5p
hsa-miR-10a-5p
hsa-miR-16-5p
hsa-miR-22-3p
hsa-miR-26a-5p
hsa-miR-941-3p
hsa-miR-21-5p
hsa-miR-10b-5p
hsa-miR-103a-3p
hsa-miR-181a-5p
hsa-miR-378a-3p
hsa-miR-191-5p
hsa-miR-100-5p
hsa-miR-182-5p
hsa-miR-29a-3p
hsa-let-7f-5p
hsa-miR-186-5p
hsa-miR-27b-3p
hsa-miR-92a-3p
hsa-let-7a-5p
hsa-miR-22-3p
hsa-miR-16-5p
hsa-miR-25a-5p
hsa-miR-10b-5p
hsa-miR-10a-5p
hsa-miR-181a-5p
hsa-miR-103b
hsa-miR-103a-3p
hsa-miR-21-5p
hsa-miR-941-3p
hsa-miR-182-5p
hsa-miR-378a-3p
hsa-miR-191-5p
hsa-miR-100-5p
hsa-miR-29a-3p
hsa-let-7f-5p
hsa-miR-27b-3p
hsa-miR-181b-5p
***
n.s.
*

Figure 11

A

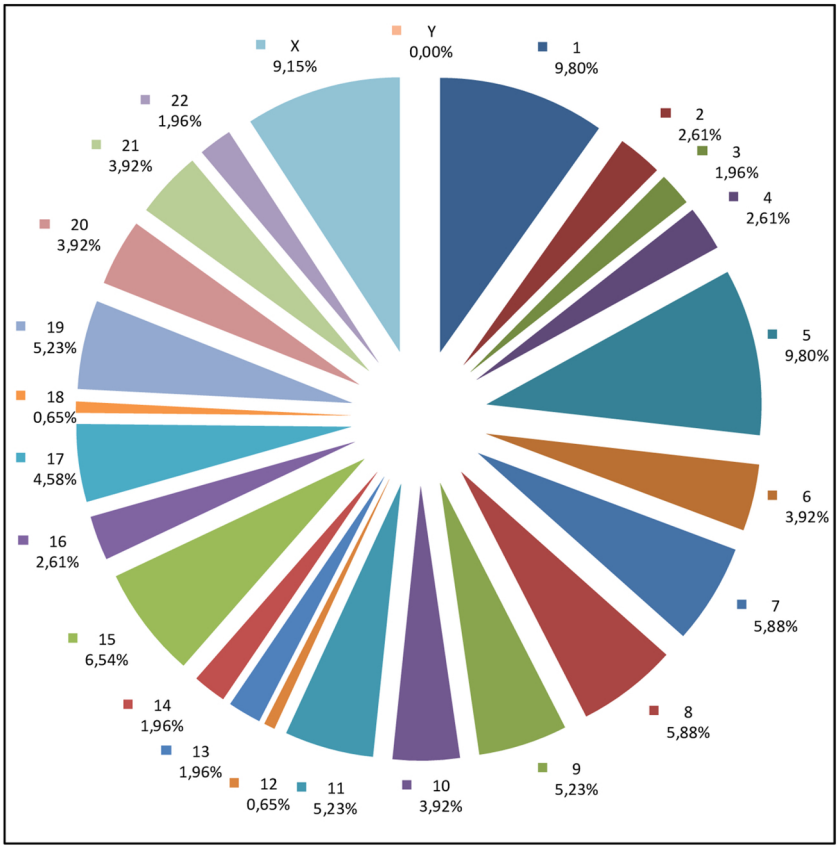
X 9,15%
Y 0,00%
1 9,80%
2 2,61%
3 1,96%
4 2,61%
5 9,80%
6 3,92%
7 5,88%
8 5,88%
9 5,23%
10 3,92%
11 5,23%
12 0,65%
13 1,96%
14 1,96%
15 6,54%
16 2,61%
17 4,58%
18 0,65%
19 5,23%
20 3,92%
21 3,92%
22 1,96%

B

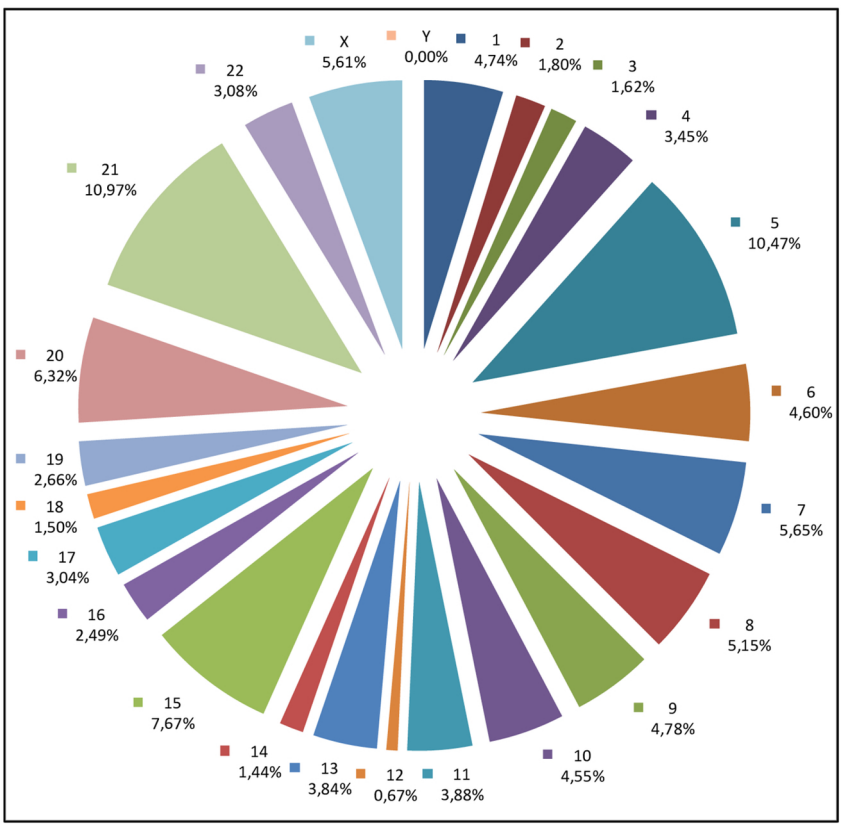
X 5,61%
Y 0,00%
1 4,74%
2 1,80%
3 1,62%
4 3,45%
5 10,47%
6 4,60%
7 5,65%
8 5,15%
9 4,78%
10 4,55%
11 3,88%
12 0,67%
13 3,84%
14 1,44%
15 7,67%
16 2,49%
17 3,04%
18 1,50%
19 2,66%
20 6,32%
21 10,97%
22 3,08%

Figure 12

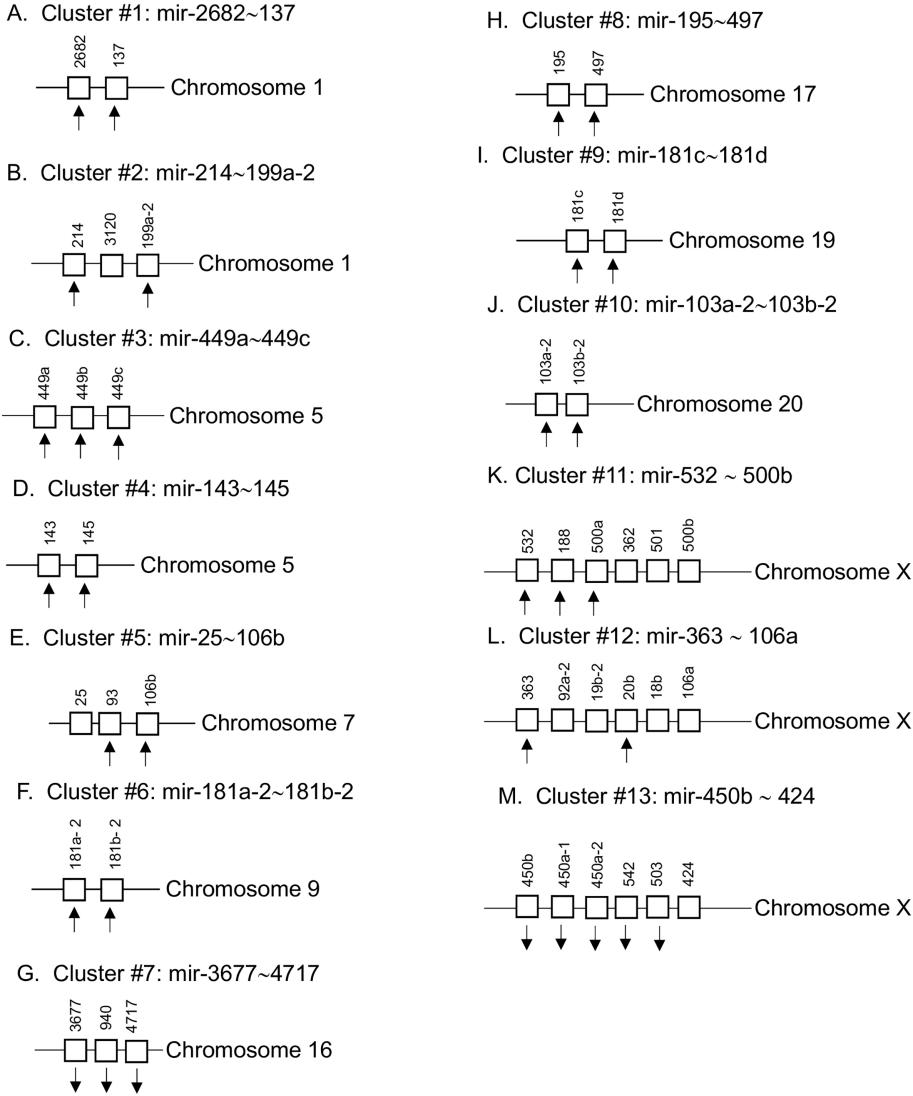
A. Cluster #1: mir-2682~137
2682
137
Chromosome 1
B. Cluster #2: mir-214~199a-2
214
3120
199a-2
Chromosome 1
C. Cluster #3: mir-449a~449c
449a
449b
449c
Chromosome 5
D. Cluster #4: mir-143~145
143
145
Chromosome 5
E. Cluster #5: mir-25~106b
25
93
106b
Chromosome 7
F. Cluster #6: mir-181a-2~181b-2
181a- 2
181b- 2
Chromosome 9
G. Cluster #7: mir-3677~4717
3677
940
4717
Chromosome 16
H. Cluster #8: mir-195~497
195
497
Chromosome 17
I. Cluster #9: mir-181c~181d
181c
181d
Chromosome 19
J. Cluster #10: mir-103a-2~103b-2
103a-2
103b-2
Chromosome 20
K. Cluster #11: mir-532 ~ 500b
532
188
500a
362
501
500b
Chromosome X
L. Cluster #12: mir-363 ~ 106a
363
92a-2
19b-2
20b
18b
106a
Chromosome X
M. Cluster #13: mir-450b ~ 424
450b
450a-1
450a-2
542
503
424
Chromosome X

Figure 13

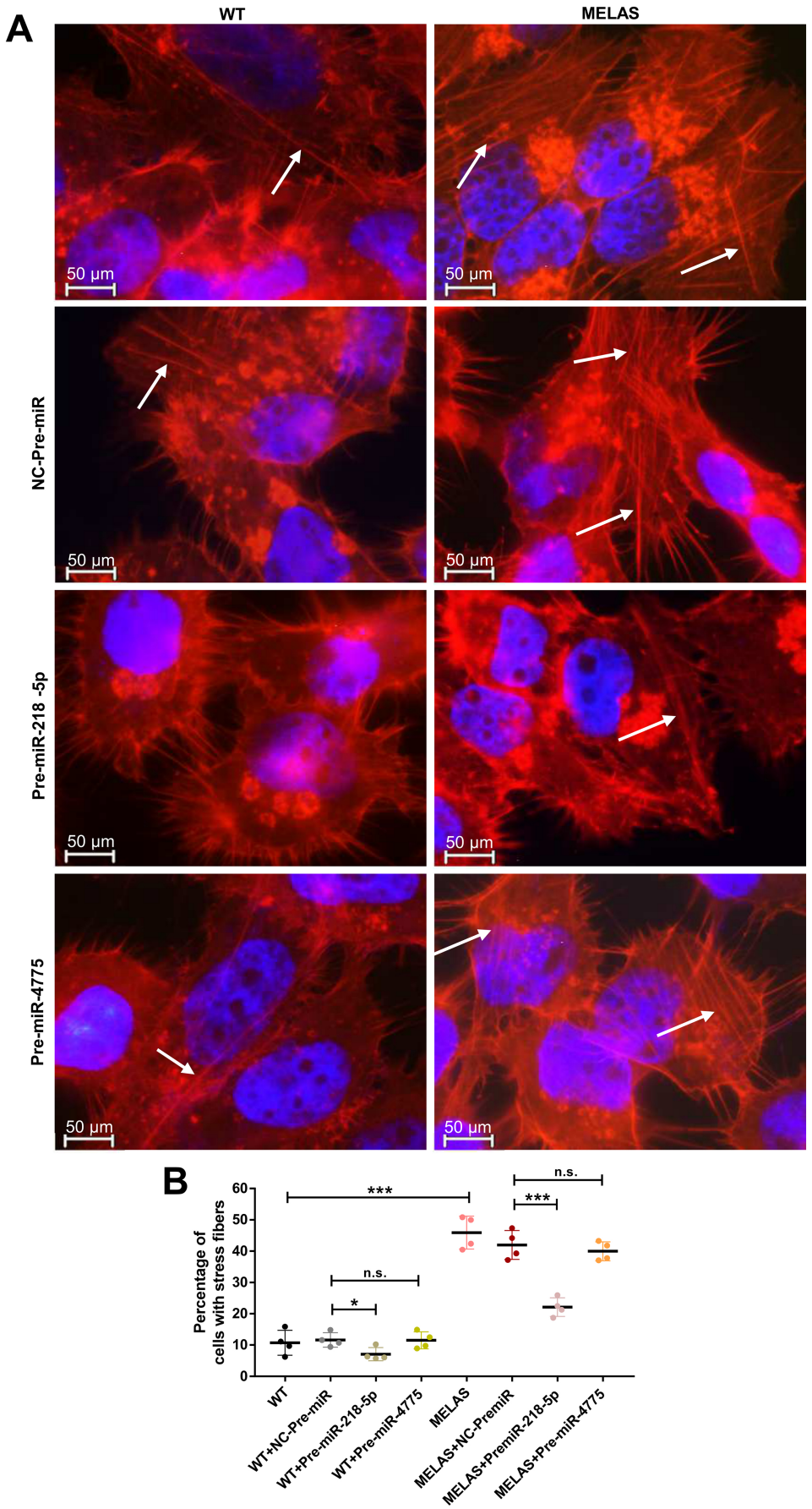
A
WT
MELAS
NC-Pre-miR
Pre-miR-218 -5p
Pre-miR-4775
50 μm
B
Percentage of cells with stress fibers
0
10
20
30
40
50
60
***
n.s.
*
n.s.
***
WT
WT+NC-Pre-miR
WT+Pre-miR-218-5p
WT+Pre-miR-4775
MELAS
MELAS+NC-PremiR
MELAS+PremiR-218-5p
MELAS+Pre-miR-4775

Figure 14